Article:
Kirkby, MJ (2014) Do not only connect: a model of infiltration-excess overland flow based on simulation. Earth Surface Processes and Landforms, 39 (7). pp. 952-963. ISSN 0197-9337

https://doi.org/10.1002/esp.3556

Do not only connect: A model of infiltration-excess overland flow based on simulation.

Mike Kirkby, School of Geography, U. Leeds, UK

Abstract

The paper focusses on connectivity in the context of infiltration-excess overland flow and its integrated response as slope-base overland flow hydrographs. Overland flow is simulated on a sloping surface with some minor topographic expression and spatially differing infiltration rates. In each cell of a 128 x 128 grid, water from upslope is combined with incident rainfall to generate local overland flow, which is stochastically routed downslope, partitioning the flow between downslope neighbours.

Simulations show the evolution of connectivity during simple storms. As a first approximation, total storm runoff is similar everywhere, discharge increasing proportionally with drainage area. Moderate differences in plan topography appear to have only a second order impact on hydrograph form and runoff amount.

Total storm response is expressed as total runoff, runoff coefficient or total volume infiltrated; each plotted against total storm rainfall, and allowing variations in average gradient, overland flow roughness, infiltration rate and storm duration. A one-parameter algebraic expression is proposed that fits simulation results for total runoff, has appropriate asymptotic behaviour and responds rationally to the variables tested. Slope length is seen to influence connectivity, expressed as a scale distance that increases with storm magnitude and can be explicitly incorporated into the expression to indicate runoff response to simple events as a function of storm size, storm duration, slope length and gradient.

The model has also been applied to a 10-year rainfall record, using both hourly and daily time steps, and the implications explored for coarser scale models. Initial trails incorporating erosion, continuously update topography and suggest that successive storms produce an initial increase in erosion as rilling develops, while runoff totals are only slightly modified. Other factors not yet considered include the dynamics of soil crusting and vegetation growth.

Introduction

Over the last ten years, the number of articles and citations for the term 'connectivity', in the contexts of both hydrology and geomorphology has increased greatly, with over thirty new articles year now published in ISI journals and over 800 citations a year in 2010-2012 (Web of Science, 2012). The concept of connectivity has been even more widespread in the ecological literature, particularly with the introduction of circuit theory, using the concept of conductance defined for all habitat and matrix areas to define potential for migration between areas for a species.

Initial concepts of connectivity have focused on the presence or absence of point-to-point connections between pairs of points (Bracken & Croke, 2007) or between regions (Bartel et al, 2011). In ecological contexts where there is no directional structure, connection between points can be powerfully extended through conductance models (McRae, 2008) but these have little applicability in hydrology, where flow is strongly directed downslope.

Connectivity between two points A and B, on a flow line, can be described as a nominal variable (presence or absence of connection), as a scalar (time delay or breakthrough volume), or as increasingly complex vectors (hydrograph at B for given input at A), even at

steady state for a conservative system. Detailed descriptions of dynamic connectivity between adjacent points across an area form one critical ingredient of fine scale process-based models, such as CRUM (Reaney et al, 2007) or MAHLERAN (Wainwright et al, 2008). In this way, connectivity provides a valuable way of conceptualizing the local persistence and continuity of overland flow, particularly in semi-arid areas with short bursts of rainfall and patchy surface properties (e.g. Cammeraat, 2002). For time-spans over which the soils and topography can respond, the division between structural and functional connectivity (Wainwright et al, 2011) is also valuable; structure providing a necessary pre-condition for functional connection, and function a conditioning set of drivers for change in structure.

To generalise response beyond the strictly local scale, it has seemed valuable to collapse the detail of overland flow connectivity into summary index variables, providing one or a few parameters that, for example, scale the response of a hillslope or small catchment to storm rainfall (e.g. Stieglitz et al, 2003, Bracken and Croke, 2007, Lane et al, 2009). Candidate indices include average travel times from runoff generating cells, average residence times and contributing areas, all potentially time-varying in response to catchment condition and storm rainfall. Although no magic bullet has yet emerged (e.g. Bracken et al, 2013) to summarize the complexity of hillslope or catchment response, it is helpful to observe, through simulations, how and why topography and soil properties influence the runoff generated from an area.

The approach taken here is to examine the connections between rainfall, applied uniformly across a heterogeneous surface, and the runoff response at the slope base. This is the integral of local connectivities that is most relevant to the way that hillslopes respond to storm events and provides a necessary basis to a better understanding of the consequent erosion patterns.

The discussion here is also focussed on the response of semi-arid areas, where runoff generation is assumed to be generated through the infiltration excess mechanism.
Storm runoff is generated here for a simulated hillslope, using a simple modified Green-Ampt infiltration equation that links infiltration rates with near-surface storage of infiltrated water, providing an interactive feedback between rainfall and soil moisture conditions. A theoretical analysis of the infiltration process in semi-arid soils does not yet provide a better simple formulation of this relationship, and the Green-Ampt approach has been operationalised through many field measurements in the Nogalte catchment in SE Spain (Dalen, 2011), providing data on appropriate values for the infiltration parameters and their large variability. This area has a Mediterranean climate, with an annual precipitation of 350-400 mm. Field work has shown no clear spatial structure for the variability (cf. Mueller et al, 2008) , for example with respect to up-slope down-slope position or drainage pathways defined by micro-topography and values here have been assumed to be random, independently sampled for each (2.5 m) grid cell.

The purpose of the model is to relate the cell-scale processes to the behaviour of the hillslope as a whole, examining the response to a range of simple storms on randomly generated surfaces of different roughness, some with no structure and others with a structure developed by erosional processes acting on an initially random surface.

Simulation Model

Initial surfaces have been generated on a 128 x 128 cell square grid, creating a pseudo-fractal surface which provides small roughness elements at all scales, and adding a general, usually uniform gradient from top to bottom of 2%. 5%, 10% or 30%. Any pits are filled in to ensure that water will flow to the slope base. For a valleyed surface, a hillslope erosion model has

been applied to this initial surface (Kirkby and Bull, 2000), applying differences in the 'effective bedload fraction' to provide alternative degrees of gully incision corresponding to different erosional pathways along the transport limited to supply limited spectrum. The scaling has been done on the assumption that each cell is 2.5 m square, so that the whole hillslope represents an area of 320 x 320 m, approximately 10 Ha. Figure 1 shows the surfaces on which runoff has been simulated, (a) for a relatively smooth un-incised surface, (b) for a surface with greater fractal roughness and (c) for a valleyed surface. In all cases the top of the slope is a divide, the bottom a base level and a periodic boundary condition laterally. Flow pathways and drainage areas are defined on these initial surfaces, allowing flow to be partitioned towards all (D8) downslope neighbours in proportion to the third power of the respective gradients. This exponent (n = 3) has been chosen to give a degree of flow convergence between very free partition (n<=1) and unique flow along the line of steepest descent (n→∞). Figure 1 (d – f) shows the corresponding distribution of catchment areas. (d) shows some flow convergence, with predominant downslope flow; (e) much greater lateral wandering of flow paths and (f) a clear structure, with smoothed divide areas and strong focussing of flow.

The modified Green Ampt equation (1911) assumes that the infiltration capacity is defined by the expression $f = A + B/S$,where

f = infiltration capacity (mm hr^{-1}),

S = near surface storage capacity (mm) and

A, B are constants.

In this formulation (Kirkby, 1976, p. 328) the storage is assumed to receive infiltrating water, and to lose water through steady leakage at rate A, through evapotranspiration, and

(rarely) through downward drainage where it exceeds a rooting depth. For infiltration into an initially dry soil, this expression is equivalent to the simplified version of the Philip (1957-8) equation,

$f = C + D\,t^{-1/2}$, where

T = elapsed time and C,D are constants with C=A and $D = \sqrt{B/2}$.

Mean values and standard deviations for the infiltration constants A and B are representative values taken from field work in the Nogalte catchment, SE Spain (Dalen, 2011), based on sprinkler and mini-disk infiltrometer measurements. Figure 2 shows the quartiles of infiltration capacity using these values and their variabilities.

To route runoff through the system, cells are processed from the highest to the lowest elevations. For each cell, previous flow from upslope is added to current rainfall, in 2 minute intervals, to determine the infiltration rate and change in storage, S, integrated over the time interval. The surplus is the runoff generated by this source cell during the time interval. This source runoff is then distributed between successive neighbouring cells. Because flow is generally able to go in more than one direction, the runoff has been apportioned stochastically, tracking a number (usually 50) of individual parcels, each a realisation of the runoff that was generated in the source cell. Each parcel is randomly allocated to a flow direction according to the respective gradients. At each step along its path, overland flow velocity is calculated as proportional to a power law of runoff depth (with exponent 1.0), inherited from the source cell, and local gradient (with exponent 0.5. These exponents provide a good approximation to the Darcy-Weisbach equation for depths of the order of the roughness elements. The overland flow constant (250 s^{-1}) is then an inverse roughness, and has been chosen to give a velocity of 1.25 cm sec^{-1} for a 1 mm depth on a 5%

gradient, a value that is consistent with previous measurements (Emmett, 1970; Holden et al 2008), although lower and higher values (60- 1250 s^{-1}) have been used for comparison. The estimated velocity is interpreted as the mean number of cells traversed in one time step, $\bar{x}$. Assuming an exponential distribution, the probability that the parcel will remain in the current cell at the end of the current time step is then $1/(1+\bar{x})$, and this outcome is decided by comparison with a random number in the range [0,1]. If the parcel does not stop, then a new onward flow direction is chosen, the original runoff depth retained, the gradient revised for the new step in the flow path, and this process is repeated until each of the 50 parcels comes to rest. Each of the destination cells (some repeatedly) then receives 1/50 of the runoff leaving the source cell, and this runoff will be passed to the destination cells, together with runoff from other up-flow source cells, for the next time interval.

Runoff has been simulated in response to simple block storms, totalling 30, 60, 75,90,120 and 180 mm falling at constant intensity for periods of 30 to 120 minutes. In all cases a uniform potential evapotranspiration of 4.1 mm day^{-1} has been applied, and this potential rate has been extracted from the storage, *S* only when there is enough, to provide a simple estimate of actual evapotranspiration.

Model behaviour

The patterns of simulated runoff that develop during the course of a storm normally show four phases, which appear to broadly match field observations. These are illustrated in relation to the overall hydrograph for a very intense storm (180 mm in 30 minutes). After a brief period during which all rainfall infiltrates, the first phase is one during which patchy runoff occurs where infiltration capacity is least, and there is little observable structure of connection between patches (figure 3a) the pattern of which largely reflects heterogeneity of

infiltration capacity. This phase lasts longer when rainfall intensities are less. In the second phase, as runoff increases, patches begin to connect into streaks of flow that are best developed where drainage area is greatest, along potential flow lines and with visibly increasing runoff downslope. This is shown for the end of the rainstorm in figure 3b. In the third phase, connections are well established and create a clearly structured flow network that takes advantage of the areas of convergence and shows a consistent increase downslope. In small storms the second and third phases may not fully develop. In the fourth phase, after rainfall has stopped, runoff ceases in a growing area from the divide, but structural connections continues to develop in the shrinking area of active runoff downslope (figures 3c and d).

The form of the output hydrograph is controlled by the balance between storm rainfall, infiltration rate and overland flow velocities. Figure 4a illustrates average slope-base runoff from rainfall at 60mm hr^{-1} for periods of 30-120 minutes, showing the build-up and decay of overland flow over time. Runoff commences shortly after the beginning of rainfall, and increases while the rain continues, initially at an increasing rate, but eventually reaching a steady state plateau value (beyond the scope shown in the figure). Once rain stops, flow follows comparable recession curves until all the remaining water is infiltrated or evaporated. Figure 4b shows the comparable evolution of flow downslope, during a single 120 mm storm. It can be seen that runoff is, to begin with, preferentially generated near the top of the slope. The upslope sections generate their peak runoff near the end of rainfall, whereas the marginal additional contribution from successive downslope sections peaks progressively later and lower, associated with the flow of runoff from upslope and the continued maintenance of strongly connected structure after rainfall has ceased.

Further insight into the behaviour of the flow is shown by tracing rainfall falling on a single line of cells near the top of the slope. The water has been traced in the simulation by assuming that, within each grid cell and time step, there is uniform mixing of overland flow and, separately, of infiltrated water as each partition flows downstream. As the tracer flows down the slope, the overland flow generated in the source cell is progressively lost to infiltration as it travels downslope, as well as being progressively delayed. At this high intensity (120 mm over 60 minutes), only a minority of the total rainfall is lost to infiltration, whereas most of the tracer water infiltrates close to where it was applied, so that the runoff coefficient for the traced water from the top of the slope is very low. Tracer applied farther down the slope shows progressively higher runoff coefficients.

Within the plots that do not have a clear drainage structure (figures 1 a and b), total simulated storm runoff at any distance from the divide is more or less constant, so that basal discharge from individual cells can be approximated as directly proportional to area, as is shown in figure 5a, which shows a slight trend for higher runoff at upslope cross-sections. The figure is drawn for a 120mm, 60 minute storm on the smoothish slope (figures 1a and 1d). Similar results and similar total runoff is obtained for the rougher slope configuration (figures 1b and 1e). The valleyed slope (figure 5b, based on figures 1c and 1f), however shows a slightly stronger, though still relatively small overall trend towards lower runoff for larger drainage areas. In addition, groups of points cannot readily be separated according to their downslope position, partly because the formation of valleys gives a much wider range of drainage areas at downslope sites (e.g. for x=112 which is at 87% of total slope length). It therefore seems relevant to compare storms, plot lengths and plot gradients on the basis of total storm runoff, recognizing that this generally differs by less than a 2:1 ratio throughout, and it is concluded

that the plan form of the slope has only a secondary impact on the total quantity of runoff generated in a storm.

The shape of the overland flow hydrograph, and the total volume of runoff generated for a given storm rainfall profile, depend on two processes that compete to remove the rain water; the rate of infiltration and the velocity of overland flow. The balance between these two processes produces two opposing effects. First, during a storm of a given size, increasing overland flow velocity (relative to infiltration) reduces the depth of surface detention but hastens its removal, so that runoff increases more rapidly while it is raining. Second, once rainfall has stopped, rapid overland flow continues to evacuate the surface water and depresses the tail of the hydrograph. At moderate velocities, the first effect predominates and total runoff volume increases with overland flow velocity, but at very high velocities, the rapid hydrograph recession begins to reduce the peak and the total runoff volume. Figure 6 illustrates this effect for a small and a larger storm. For the 30mm storm (a and c) the first effect predominates almost throughout, whereas for the 120mm storm (b and d), the depression of the hydrograph tail becomes dominant for more rapid flows. Combining figures 6(a) and (b), the second effect predominates roughly in the zone for which (total runoff) x (overland flow parameter) > a constant(~ 4000 mm. s^{-1}), and this cross-over point is maintained for runs with increased or reduced infiltration rates. At upslope slope positions, flow depths and therefore overland flow velocities are less than downslope, so that runoff builds up more rapidly reaching higher totals for any given overland flow parameter. As will be seen below, the balance between infiltration and overland flow rates also influences the way in which runoff responds to differences in slope gradient down the slope profile.

Figures 6(a) and (b) also show the effect of slope length on runoff. Below the cross-over point, there is a clear decrease in runoff with increasing slope length. Above it, runoff is approaching a state of equilibrium in which most rainfall runs off, and the effect of slope length is much less marked.

Aggregate storm runoff

Comparing storms of different rainfall totals, the first order model of storm response suggests a clear runoff threshold, with little runoff for storms below the threshold and an almost linear increase in runoff above it, corresponding to a constant fraction (asymptotically approaching 100%) of additional rainfall. This pattern is repeated with minor variations, as storm duration or gradient is altered. Figure7(a) shows this overall behaviour for simple storms of 30 – 180 mm and on gradient of 2% -30%, for the smoothish surface (figures 1a and 1d). Runoff is shown here for the base of the slope, and for a constant overland flow parameter. It can be seen that the runoff threshold is only secondarily sensitive to variations amongst the parameters shown. For practical runoff modelling, where inputs and parameters are not generally as well constrained as in a simulation model, this simple threshold model may be the best that can be achieved, and has the advantage of greatest reliability for the largest and most significant events.

However, closer examination of figure 7(a) shows, as is to be expected, that there is always some runoff from patches of low infiltration adjacent to the slope base, even with small storms of low intensity, associated with the spatial variability in infiltration rates. It is therefore instructive to look more closely at the form of the response around the apparent threshold, since many natural storms fall in this region, and to compare the sensitivity of this elbow region to the key driving variables. In figure 7(b) the data shown in figure 7(a) are re-plotted as runoff coefficients on log-log scales. This expands the elbow region and the straight-line segment of figure7(a) is converted into the upper zone where runoff levels off towards 100% of rainfall. Very similar curves can be generated for responses to differences in the overland flow parameter (25%-400% of standard values) and in the infiltration rate (50%-200% of standard values). In all cases there is an almost straight-line increase in the

log-log plot, approximating a power law response for the elbow region. The slopes of these lines are similar, suggesting that the runoff coefficient is proportional to storm runoff to the power of 3-4. For zero rainfall this power law relationship is consistent with the physical requirement of zero runoff.

Figure 7(c) shows a third way of summarising the same dataset for storms of 30 minute duration, plotting total end-of-storm Infiltration (= Rainfall – Runoff -Evaporation) against total storm rainfall, on arithmetic scales. For small storms, there is negligible runoff and infiltration equals rainfall. For the largest storms there is an inverse relationship in which infiltration behaves like an inverse power (<=1) of storm rainfall. This reduction is due to the partition of rainfall between infiltration and overland flow. On steeper gradients, with consequently increasing overland flow velocity, the transition to this decline in response occurs sooner and the maximum volume infiltrated during a storm is less.

A simple algebraic expression has been fitted to the form of these runoff and total infiltration curves. It takes the form:

$$r = \frac{R}{1+(R_0/R)^3} \quad (1)$$

$$F = R - r = R\left[1 - \frac{1}{1+(R_0/R)^3}\right] = \frac{R}{1+(R/R_0)^3} \quad (2)$$

where r is the total storm runoff in mm,

F is the total volume of infiltrated water during the storm,

R is the total storm rainfall in mm

and R_0 is a constant rainfall threshold in mm.

Equation (2) behaves like $F=R$ for small values of R, with almost all rainfall infiltrating, and like $F = R^{-2}R_0^3$ for large values of R. Ignoring the (very small) evaporation, the runoff

coefficient $p=r/R$ behaves like $p = (R/R_0)^3$ for small R, corresponding to the approximate power law relationship apparent in figure 8(b). At large rainfalls, equation (2) approaches p=1 asymptotically, so that equations (1) and (2) behave appropriately for both small and large values of storm rainfall. This power law behaviour for small rainfalls is interpreted as a response to the spatial variability in infiltration rates, with small amounts of runoff generated from low-infiltration areas close to the lower boundary.

The maximum seen in figure 7(c) can be obtained from equation (2) by differentiation, giving the maximum at $R_{max} = R_0.2^{-1/3}$, taking the value (3)

$$F_{max} = {}^{2}/_{3}\ R_{max} \quad (4)$$

The locus of maxima therefore lies on a straight line through the origin.

Figure8(a) shows curves comparable to figure 7(c) for variations in infiltration rate; figure 8(b) for variations in the overland flow velocity parameter and figure 10(a) for variations in storm duration. The effect of these three variables can be adequately fitted to equation (1) with the single parameter R_0.

Table 1 shows the approximate values of the R_0 parameter as one variable at a time is altered. Using these parameter values, the data points shown in figures 8(a) and 8(b), together with data for storm duration have been re-plotted, comparing the values of the algebraic expression , equation(1), with the values obtained from the detailed simulations, and showing moderately good overall agreement. The data values shown in figures 8(a),8(b) and 10(a) are compared in figure 8(c) with the algebraic form, using the parameter values of table 1, showing a good level of overall agreement. Interpreting these relationships, in which variables have been modified independently, one at a time, the parameter R_0 can be seen as a measure of both the slope gradient and the storm duration. R_0 can then also be shown to

increase, as might be expected, with increases in infiltration capacity and with decreases in the overland flow parameter. In considering the balance between infiltration and overland flow processes, infiltration rate and storm duration promote the former; and gradient and overland flow parameter promote the latter. The dependence of the R_0 parameter on gradient and storm duration can be obtained from regression as

$$R_0 = 36.6 - 32.3\, log_{10}\, G + 0.51\, T, \qquad (5)$$

where G is tangent gradient and T is storm duration in minutes, with $r^2 = 0.987$.

Connectivity structure

Very little of the rainwater originally falling near the top of the slope actually reaches the slope base before being lost to infiltration or evapotranspiration, so that connectivity between this rainfall site and the slope base is very weak. Application of tracer in rainfall applied successively farther downslope shows that progressively less of the traced rainfall is lost. The most natural stochastic model is perhaps to assume an exponential decline so that movement from the source approximately follows a Poisson process, in which the probability of infiltration for surviving runoff is constant per unit distance. A better, though far from perfect fit to the simulation data is, however, provided by the relationship:

$$\Pi(x) = 1/\left(1 + {}^{x}/_{X}\right)^2 \qquad (6)$$

where x is distance downslope from the injection point,

$\Pi(x)$ is the probability that water will go farther than x,

assuming 100% runoff coefficient for the source cell,

and X is the scale distance, associated with the probability 2/(x+X) as the (marginal) probability of infiltration loss per unit distance for the water that has not yet infiltrated.

Summing over rain falling at all points along a slope of length L,, the total probability of runoff, that is the runoff coefficient, is obtained by integration of equation (6) over all shorter path lengths, to give

$$p(L) = \frac{1}{L}\int_0^L \Pi(x).dx = 1/(1 + L/X) \quad (7)$$

Equation (7) provides an explicit relationship between the runoff coefficient and slope length, for a particular storm, with maximum runoff for short slopes and steadily decreasing as length increases. Figure 9 shows examples of curves obtained for the full simulation, closely conforming to equation (7) and Table 2 shows estimated values of the estimated scale distance for a range of storms, showing variations over more than two orders of magnitude that vary most strongly with storm total rainfall.

If the scale distance defined here is greater than the length of the slope, then the whole hillslope is contributing significant runoff, and the runoff coefficient begins to increase towards its asymptotic value of 100%. Comparing this approach with the analysis using equation (1), and illustrated in figure 7(b) above, the threshold R_0, near which runoff approaches 100%, can be interpreted as the storm rainfall at which the scale distance becomes equal to the slope length, and the fall-off in runoff below that as the effect of reducing scale lengths and associated contributing areas.

Equations (1) and (7) can now logically be combined. Following equation (1), the relevant values of R_0 have been obtained for the fixed slope length of 320 m. For this length, referred to here as L_0, both equations (1) and (7) should be valid, in the form

$$p = \frac{r}{R} = \frac{1}{1+\left({}^{R_0}/_{R}\right)^3} = \frac{1}{1+{}^{L}/_{X}} \quad (8)$$

with notations as before, except that R_0 should now be specifically associated with a particular "standard" slope length L_0, in this case the 320 m slope length used in most of the simulations reported here. Combining these equations gives the more general form:

$$p = \frac{1}{1+\frac{L}{L_0}\left(\frac{R_0}{R}\right)^3} \quad (9)$$

which combines the two approaches. It follows that, for a given storm rainfall R, the scale distance of connectivity

$$X = L_0 \left(\frac{R}{R_0}\right)^3 \quad (10)$$

and that, for a given slope length L, the associated rainfall threshold parameter

$$R = R_0 \left(\frac{L_0}{L}\right)^{1/3} \quad (11).$$

The simulations presented here suggest that, for a semi arid area, the infiltration excess overland flow at any point depends on the localised convergence of catchment area within the (variable) scale distance of connectivity which depends on storm magnitude. For all but the largest events, flow is generated patchily within a catchment, and the threshold for catchment-wide floods is set by establishing connectivity between the majority of hillslopes and the channelways. When a storm is large enough for the scale distance to exceed the average slope length (the reciprocal of twice the drainage density), most hillslopes will generate connected overland flow and most channels will then begin to flow As the connected length increases, the overland flow hydrograph persists for longer after rainfall stops, because of the time taken for flow to travel from the most distant connected points upslope to the slope base. The combination of greater total runoff volume and increased flow duration together provide the basis for a fully connected catchment-wide flood. Within a catchment with variations in slope length and gradient, the relationships of equations (5) and (9) show that runoff is preferentially generated from areas of high drainage density and steep slopes, for example those found in badland and gullied areas.

This contrasts with behaviour in a humid area, for which the saturated contributing area is loosely related to the topographic index (the ratio of total catchment area to local gradient) and saturation excess overland flow is concentrated on downstream areas of low gradient, with the threshold for contribution primarily set up by antecedent conditions.

Some additional factors and conclusions

(i) Slope profile form

Although it has been seen above that the runoff hydrograph from a simple storm is only secondarily dependent on the plan form of the slope, and that the form of the total infiltration curve conforms to a simple algebraic form with only one changing parameter as storm duration, gradient and overland flow velocity are varied, nevertheless it has been found that there is strong sensitivity to the form of the slope profile. Figure 10 compares the total infiltration curves as storm duration is varied for respectively uniform (figure 10a), convex (b), concave (c) and convexo-concave (d) profiles, all with an average overall profile of 5%. These curves depart somewhat from the form of equation (1) above, perhaps towards

$$r = R \Big/ \left[1 + \left({}^{R_0}/_{R}\right)^{n}\right] \qquad (12)$$

with the exponent *n* lying between 1.0 and 3.0. The way in which these infiltration curves develop may be seen by comparing figure 11 with figure 4(b) above. For the uniform slope used to generate figure 4(b), successively downslope sections of the slope generate marginal runoff that is both delayed and attenuated. In figure 11(a), the convex profile shows a similar pattern, whereas the concave(figure 11b) and convexo-concave (figure 11c) profiles shows progressive delay in the onset of runoff in the concave area but with less marked attenuation. The similarity of overall response between the convex and uniform profiles is seen as a balance between the more rapid delivery of runoff downslope due to the steepening

gradient, with accelerating overland flow, and the increased removal of water from downslope areas after rainfall ceases, again due to the increased gradient and more rapid overland flow. In contrast, profiles with a concave base show slowing of overland flow, so that water remains on the surface for longer, and is able to continue infiltrating. These simulations suggest that slope profile form has a greater control on runoff dynamics than slope plan form, which was seen above to have only a second order effect.

(ii) Coarse-scale estimates of runoff

In order to apply the results of these simulations to provide runoff estimates at coarser temporal and spatial scales, and with more realistic rainfall profiles, a ten –year tipping bucket record of rainfalls for the Nogalte catchment (for which the infiltration measurements were made) has been used within the spatial model at a temporal resolution of one hour, using the initial 'standard' parameter values. The results of this simulation are shown in figure 12. In (a) cumulative rainfall and cumulative simulated runoff are plotted for the entire 10-year period. Figure 12(a) also shows runoff simulated using the same parameters, but with daily time steps. It can be seen that the daily time step generally decreases the runoff estimates, and that this difference is most marked in the largest observed events. Figure 12(b) confirms this generalisation, showing greater detail for a single major storm period (Sept-Oct 1997). Figure 12(c) plots individual daily rainfalls against the simulated daily runoff, summed from hourly time steps for each 24-hour period. It may be seen that there is a general positive relationship with some predictive potential. It should be noted that, in this log-log plot, many of the runoff values are very small. Predictive power is therefore most valuable for the larger events.

Alternatives to the use of individual daily rain totals were considered in this analysis. In particular exponentially weighted sums of successive rainfalls were tried, with a range of time decay constants, for both hourly and daily time steps. These measures, that give some weight to antecedent conditions, were. However, only marginally better as predictors of runoff. It is possible that, for a less arid area, such measures might be more advantageous.

In figure 12 (c) an additional curve has been drawn, following the form of equation (1) above, expressed in the appropriate form for total storm runoff (and identifying storm total runoff with daily rainfall totals). Curves have been drawn for a rainfall threshold of R= 70 mm. The criteria used to fit these values were first to fit the general form shown in figure 12(c), particularly for the larger events, and second to provide a correct estimate of the total simulated runoff (using the daily sum aggregated from hourly time steps) over the ten-year period. Values from these estimates based on daily rainfall, using Equation (1), are also shown in figures 12(a) and (b).

(iii) Further dynamic interactions

In the above simulations, the soil surface and its infiltration parameters have been held constant during the course of the simulations. It is recognised that there are significant changes over time, both within storms and over longer periods. The most rapid of these changes is the evolution of crusting on an unprotected surface, which greatly reduces infiltration rates from those on, for example, a freshly tilled surface. A second series of changes occurs as sediment is selectively removed from the surface by water erosion. Figure 13 shows the results of a simulation on an initially smoothish surface, through a series of ten identical large storms, each of 180 mm over 60 minutes. In the simulation the surface

topography has been adjusted to account for sediment transport after each time step, and the time steps varied dynamically to maintain computational stability. (a) shows the development of distinct rill-like channels which modify the initial surface, similar to that shown in figure 1 (a) and (d). Figure 12 (b) shows the runoff and sediment response in the first five of these storms. It can be seen that, in accordance with results reported above, the changes in plan form make only minor changes in the amount of runoff, although the improving network structure allows runoff to peak earlier in each event. However, sediment transport increases greatly as drainage network evolves, eventually levelling off in this example as improved connectivity is compensated by the decreasing gradient at rill outlets (and this is a result of the fixed basal boundary condition used here). These erosional dynamics evolve both within a single storm and over a series of storms, and may in practice be partly countered by tillage operations and natural processes (e.g. Schumm, 1956) that destroy rills between storm events.

A more subtle dynamic process, and one that has not been investigated, may accompany crusting and erosion through the evolution of spatial structural patterns for infiltration parameters. Crusting provides a mechanism for reducing inter-rill infiltration, and selective transportation of material may lead to increases in infiltration rate downstream along rill pathways. Another important process is vegetation change. Growth follows seasonal cycles and responds to the availability of soil moisture through a series of rainfall events, as well as interacting with cultivation, fire and grazing.

(iv) Provisional conclusions

It is recognised that the simulations presented here explore only one aspect of the interactions between rainfall, runoff and consequent erosion. It is not generally practicable to make

measurements on the scales simulated here, so that the simulations provide a method to explore some of the often complex and contradictory relationships between rainfall and runoff. In particular simulation provides a way of understanding how the effects of gradient, roughness, infiltration capacity and topography in plan and profile are expressed in the rainfall-runoff relationship at a scale that can be incorporated into a catchment model.

It has been shown above that, from the reasonable assumptions made, it is possible to generate a plot-scale rainfall-runoff relationship (equation 9) that has a simple structure, parameters that can be estimated from a metre-scale simulation such as that illustrated here, behaves realistically under extreme conditions and may out-perform alternative simple runoff estimators.

References cited

Bartel H., J. Van Nieuwenhuyse, M.Antoine, G. Wyseure and G. Govers, 2011. Pattern-process relationships in surface hydrology: hydrological connectivity expressed in landscape metrics. Hydrological Processes, **25**, 3760-3773.

Bracken, L.J. and Croke, J., 2007. The concept of hydrological connectivity and its contribution to understanding runoff-dominated geomorphic systems. Hydrological Processes **21**, 1749-1763.

Bracken, L.J., J. Wainwright, G.A. Ali. D. tetzlaff, M.W. Smith, S.M. Reaney, A.G. Roy 2013. Concepts of hydrological connectivity, research approaches, pathways and future agendas. Earth Science Reviews 119, 17-34.

Cammeraat, L.H., 2002. A review of two strongly contrasting geomorphological systems within the context of scale. Earth Surface Processes and Landforms, **27**, 1201-1222.

Dalen, E.N., 2011. Factors influencing runoff generation, and estimates of runoff in a semi-arid area, S.E.Spain. Unpublished MPhil thesis, University of Leeds.

Emmett, W.W., 1970. The hydraulics of overland flow in hillslopes. U.S.G.S. Professional Paper 662A, 68pp.

Green, W.H. and G.A. Ampt, 1911.Studies in Soil Physics I. The flow of air and water through soils. J. Agric Soils, **4,** 1- 24.

Holden,J., M. J. Kirkby, S. N. Lane, D. G. Milledge, C. J. Brookes, V. Holden, and A.T. McDonald, 2008. Overland flow velocity and roughness properties in peatlands. Water Resources Research,. **44**, W06415, doi:10.1029/2007WR006052

Kirkby, M.J. 1976. Implications for Sediment Transport, p 325-363 in Kirkby, M.J. (Ed) Hillslope Hydrology. John Wiley, Cheichester.

Kirkby M.J. and L.J. Bull, 2000. Some factors controlling gully growth in fine grained sediments: A model applied to south-east Spain. Catena, **40** (2), 127-46

Lane, S.N., S.M. Reaney, A.C. Heathwaite, 2009. Representation of landscape hydrological connectivity using a topographically driven surface flow index. Water resources Research 45, W08423.

McRae, B.H., B.G. Dickson, T.H. keitt, V.B. Shah, 2008. Using Circuit Theory to model connectivity in ecology, evolution asnd conservation. Ecology 89, 2712-2714.

Mueller, E.N., J. Wainwright, A.J. Parsons, 2008. Spatial variability of soil and nutrient characteristics of semi-arid grasslands and shrublands, Jornada Basin, New Mexico. Ecohydrology 1, 3-12.

Philip, J.R., 1957-58. The theory of infiltration. Soil Sci., **83**, 345-257; 535-448: **84**, 163-177; 257-264: **85**, 278-286; 333-337.

Reaney ,S.M., Bracken, L.J. and Kirkby, M.J., 2007. Use of the connectivity of runoff model connectivity in semi-arid areas. Hydrological Processes., **21 (7).** 894-906.

Stieglitz, M. J. Shaman, J. Mcnamara, V. Engel, J. Shanley, G.W. Kling, 2003. An approach to understanding hydrologic connectivity on the hillslope and the implications for nutrient transport. Global Biogeochemical Cycles 17, 1105, doi:10.1029/2003GB002041

Wainwright, J., A.J. Parsons, E. N. Müller, R.E. Brazier, D. M. Powell and B. Fenti, 2008. A Transport-Distance Approach to Scaling Erosion Rates: 1. Background and model development. Earth Surface Processes and Landforms, **33**, 813-826.

Wainwright, J., L. Turnbull , T. G. Ibrahim, I. Lexartza-Artza, S. F. Thornton and R. E. Brazier, 2011. Linking environmental régimes, space and time: Interpretations of structural and functional connectivity. Geomorphology**, 126**, 387-404.

Web of Science, 2012: Thomson Reuters

Gradient (%)	Duration (min)	ofv rate (sec^{-1})	Infiltration ratio (%)	Best fit R_0 (mm)	RMS error (mm)	Associated figure
2%	30	250	100	109	1.15	fig 7
5%	30	250	100	95	2.39	fig 7
10%	30	250	100	88	3.41	fig 7
30%	30	250	100	78	4.71	fig 7
5%	60	250	100	110	2.24	fig10a
5%	90	250	100	126	2.08	fig10a
5%	120	250	100	141	2.17	fig10a
5%	60	250	50	71	1.57	fig 8a
5%	60	250	200	172	1.68	fig 8a
5%	60	62.5	100	164	2.06	fig 8b
5%	60	1250	100	86	6.44	fig 8b

Table 1:

Approximate values of storm response parameter R_0, for total runoff at the slope base (320m).

For a given total storm rainfall, total storm runoff, r is given by the expression.

$$r = \frac{R}{[1+(R_0/R)^3]}$$

The RMS error is calculated by comparing simulated total infiltration (= R-r) with that derived from the expression, for total storm rainfalls of 30,45,60,75,90, 120 & 180mm.

Table 2. Scale travel distances for infiltration downslope.

Storm Volume (mm)	Duration (minutes)	Gradient %	Scale Distance (m)
30	60	5	4.0
60	60	5	30
120	60	5	250
180	30	5	625
30	30	5	7.5
90	90	5	70
120	120	5	125
60	60	1	16
60	60	2	22.5
60	60	10	42
60	60	20	57

Figure captions

1: Slope surfaces used for 128x128 simulations: contour maps (a-c): catchment areas (d-f).(a) and (d) represent the 'smoothish' surface: (b) and € the 'Rough' surface; (c) and (f) the 'valleyed' surface.

2: Cumulative infiltration values used in simulations, based on field measurements for SE Spain

3: Stages in runoff evolution during and after a rain event (180 mm from times 30-45). Blank areas have no flow.(a) t=34: (b) t=45: (c) t=60: (d) t=100 minutes.

4(a): Example of runoff evolution over time: Hydrographs of slope-base runoff for rainfall at 60mm/hour of differing durations

(b): Example of runoff contributions over space from each section of the slope:
120 mm storm over 60 minutes (intervals 30-60) on planar slope

5.: Total storm runoff (mm) from a 120 mm, 60 minute storm expressed in relation to area drained, at various distances in cells from the divide on (a)the smoothish surface; (b) the valleyed surface

6. Response of simulated overland flow to differences in overland flow velocity parameter (in units of s^{-1}). (a) and (b) show differences in total runoff and with slope position. (c) and (d) show differences in hydrograph form. (a) and (c) are for a 30 mm, 60 minute storm: (b) and (d) for a 120mm, 60 minute storm.

7. Dependence of total slope base storm runoff on storm size for various gradients in simulated 30 minute storms. The results are expressed as (a) Total storm; (b) Runoff coeffieient and (c) total volume infiltrated.

8. Total storm infiltration for 30 min storms of various sizes, as (a) infiltration rate and (b) overland flow velocity vary. (c) compares simulated infiltration volume with equation (1),

using parameter values shown in Table 1. Legend refers to source of variation within each group.

9. Examples of connectivity relationships between slope length and simulated runoff for 60 minute storms, closely conforming to the form of equation (6)

10. The relationship between simulated total volume infiltrated and storm volume, illustrating the influence of slope profile form and storm duration. (a) Uniform gradient (b) convex profile (c) concave profile (d) convexo-concave profile.

11. Example of runoff contributions over space from each section of the slope for a 120 mm, 60 minute storm (time intervals 30-60) on (a) convex slope, (b)concave slope (c) convexo-concave slope.

12. (a) Simulated runoff for 10-year period of observed rainfall, using hourly and daily time steps. (b) Expansion of simulated runoff for a 20-day storm period within the 10-year period, using hourly and daily time steps. (c) Relationship between daily rainfall totals for 10-year record, and daily sums of simulated hourly runoffs. Curve shows fitted algebraic expression of equation (1).

13. The impact of repeated 180 mm, 60 minute storms, allowing overland flow and rainsplash to erode the initially smoothish surface. Channelling concentrates the flow, but may also reduce gradients near the channel outlets (a) the surface after erosion by 10 storms. (b) b)Basal runoff hydrographs and sediment transport for the first six storms. Subsequent storms show similar patterns to the final storm shown here. The initial step increase in sediment at the start of each storm is due to rainsplash.

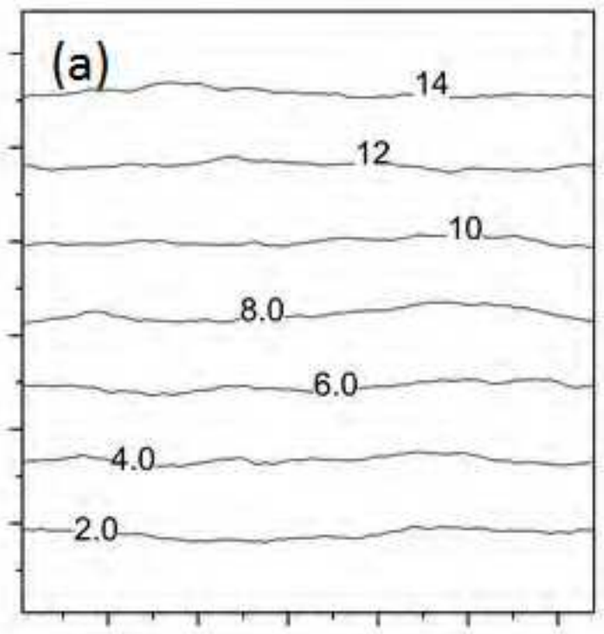
(a)
14
12
10
8.0
6.0
4.0
2.0

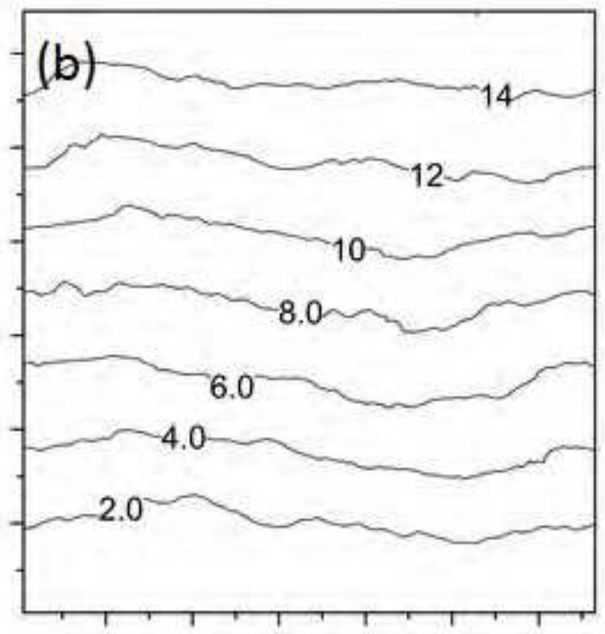
(b)
14
12
10
8.0
6.0
4.0
2.0

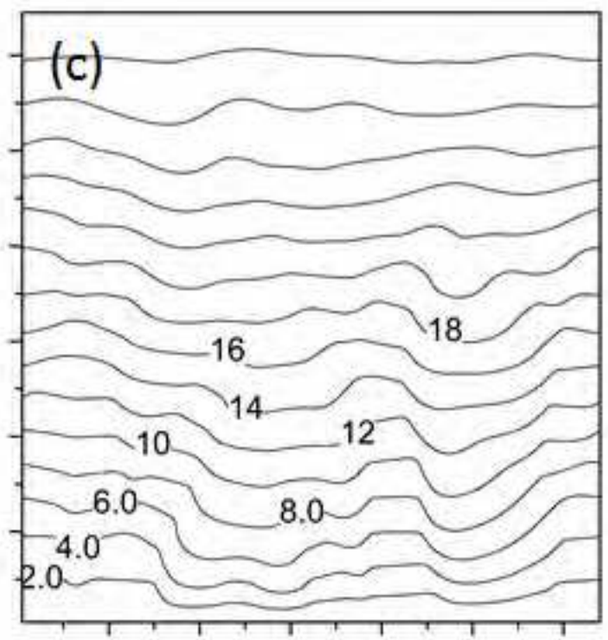
(c)
18
16
14
12
10
8.0
6.0
4.0
2.0

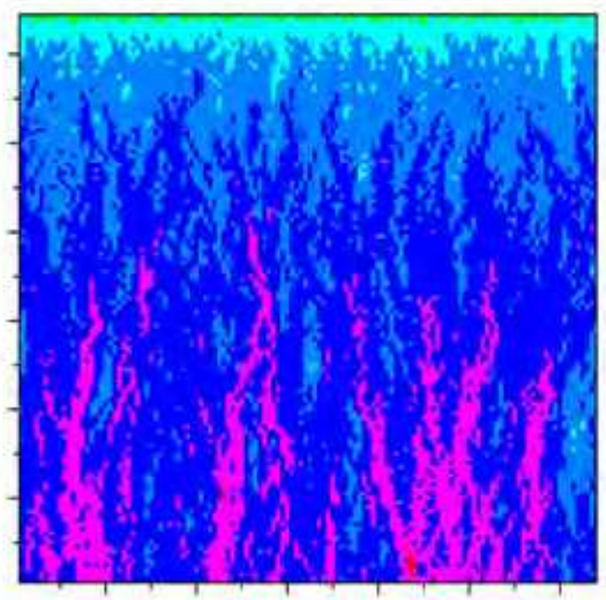

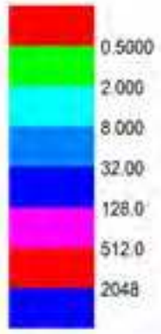
0.5000
2.000
8.000
32.00
128.0
512.0
2048

(d)

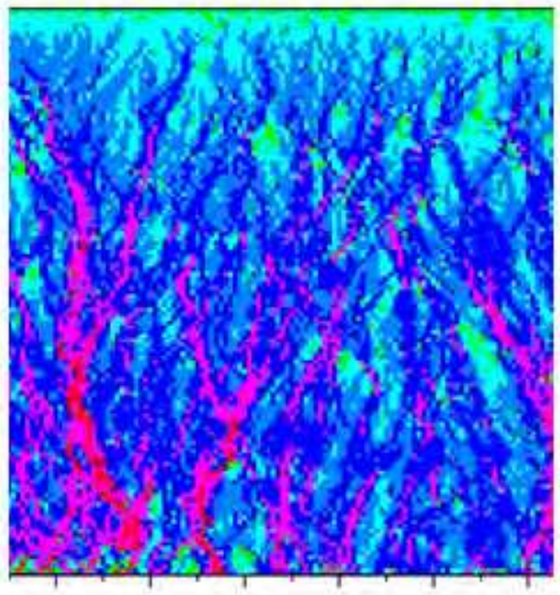

(e)

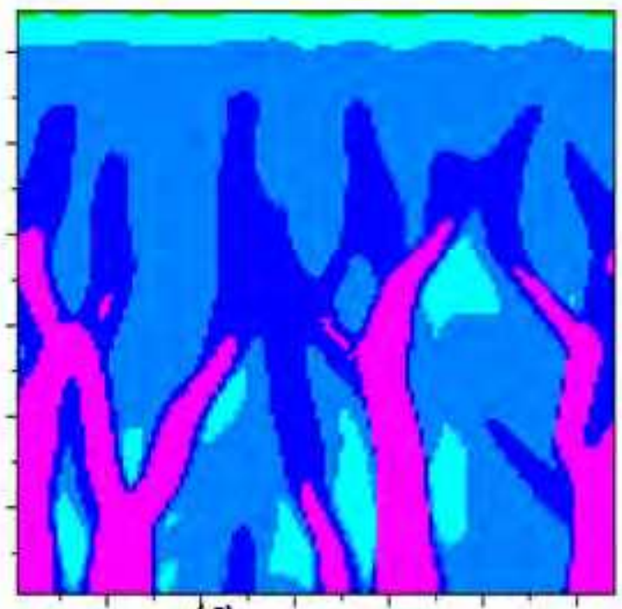

(f)

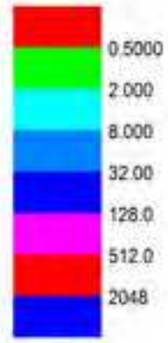
0.5000
2.000
8.000
32.00
128.0
512.0
2048

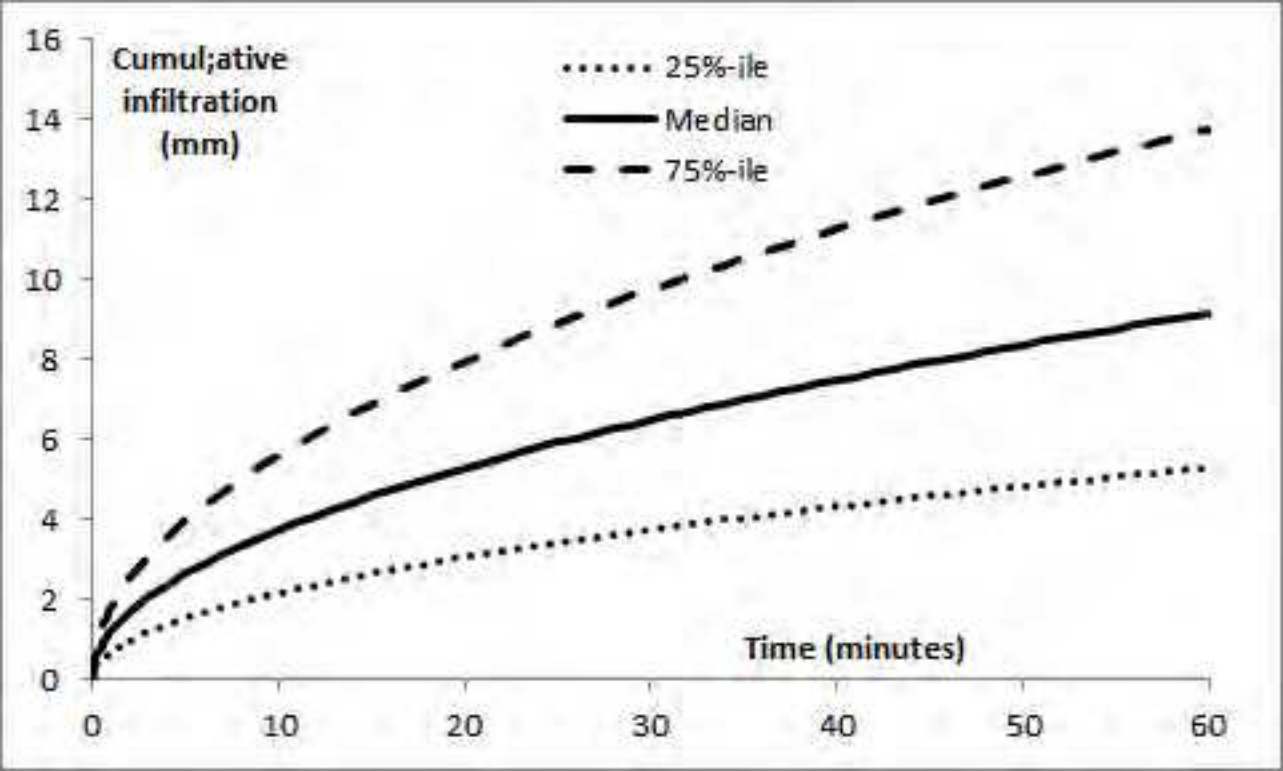
Cumul;ative infiltration (mm)
25%-ile
Median
75%-ile
Time (minutes)
0
2
4
6
8
10
12
14
16
0
10
20
30
40
50
60

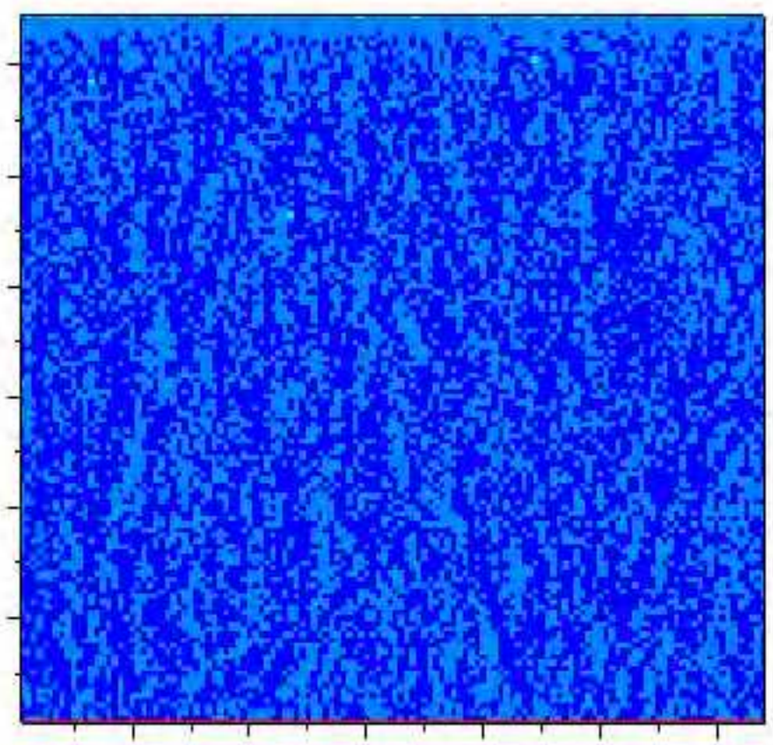

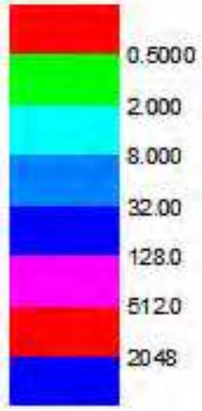

(a) t=34

(b)t= 45

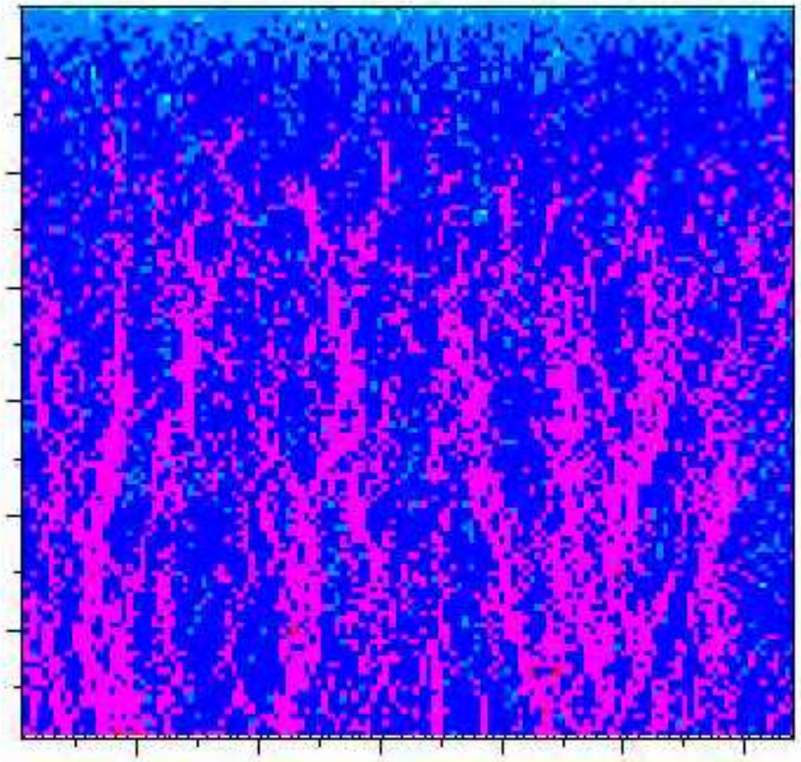

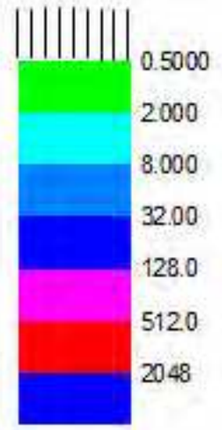

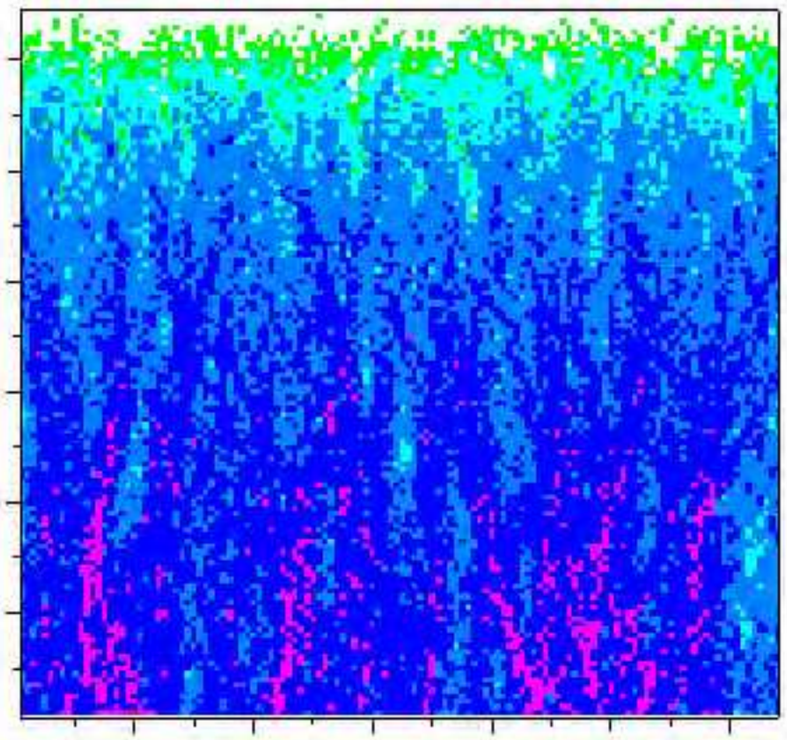

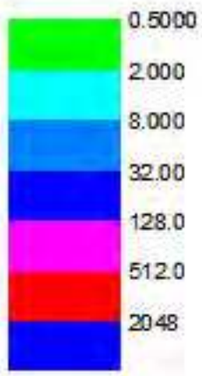

(c) t=60

(d) t=100

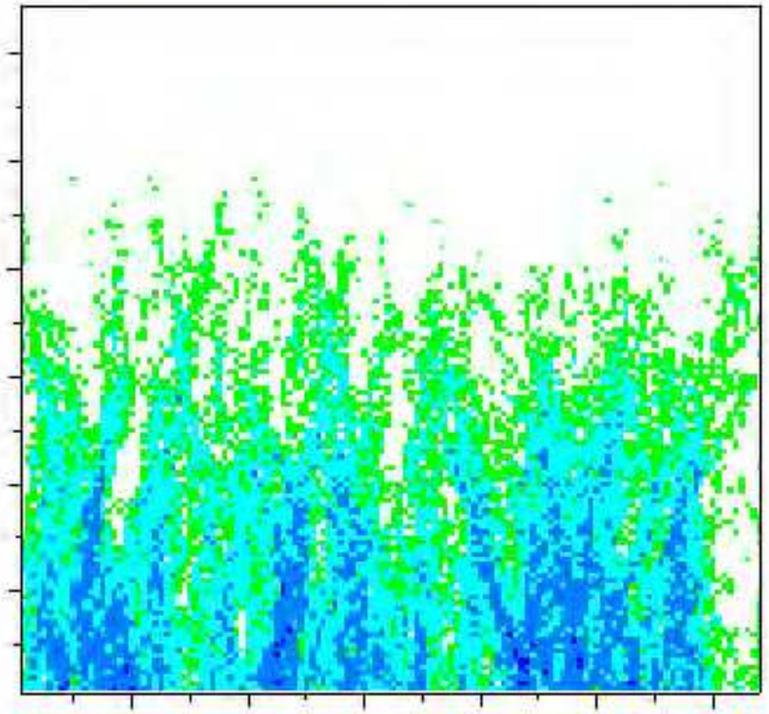

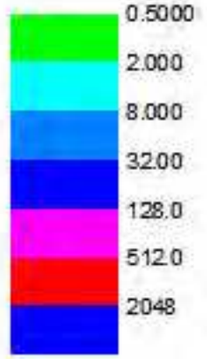

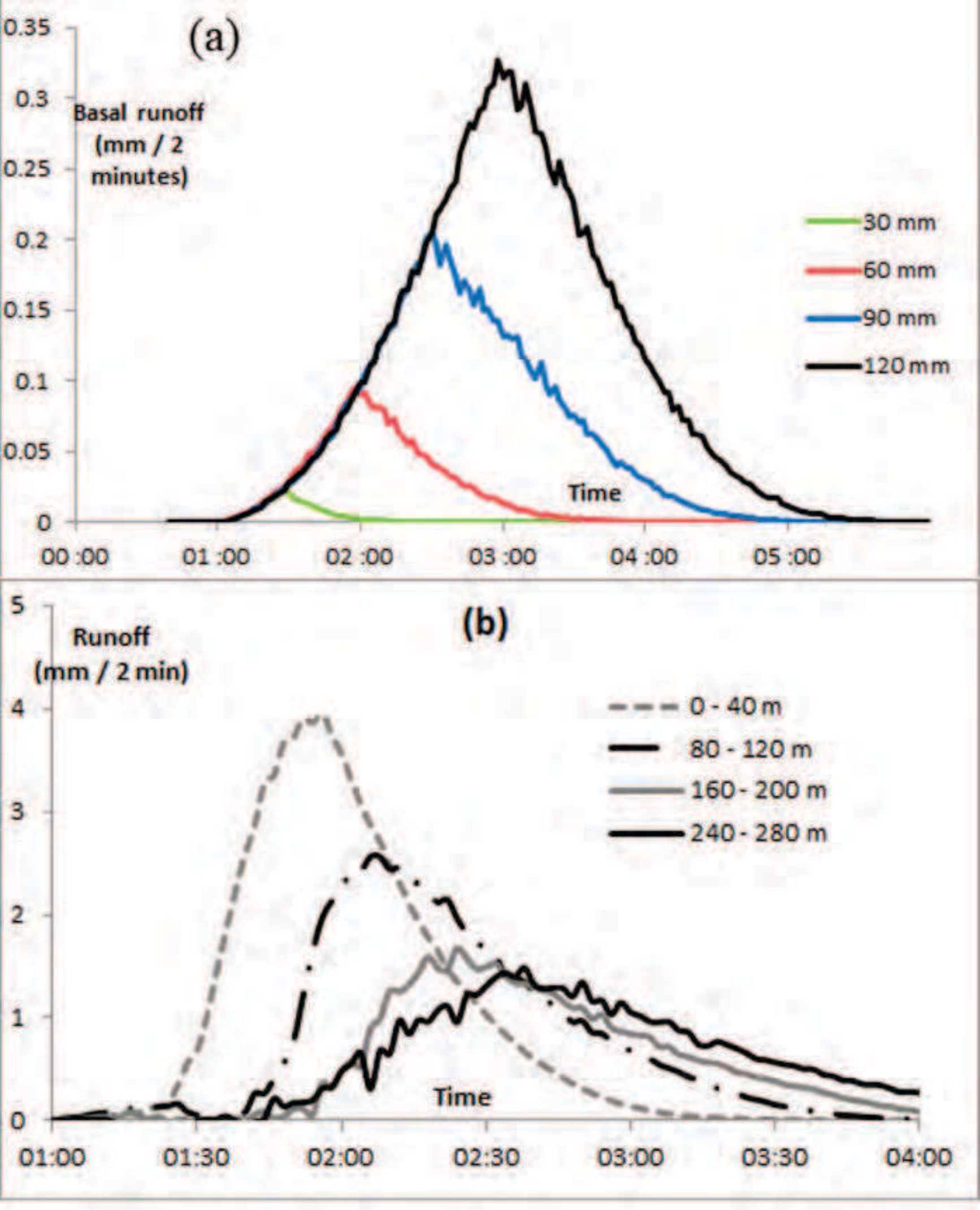
(a)
Basal runoff (mm / 2 minutes)
0.35
0.3
0.25
0.2
0.15
0.1
0.05
0
Time
30 mm
60 mm
90 mm
120 mm
00 :00
01 :00
02 :00
03 :00
04 :00
05 :00
(b)
Runoff (mm / 2 min)
5
4
3
2
1
0
Time
0 - 40 m
80 - 120 m
160 - 200 m
240 - 280 m
01:00
01:30
02:00
02:30
03:00
03:30
04:00

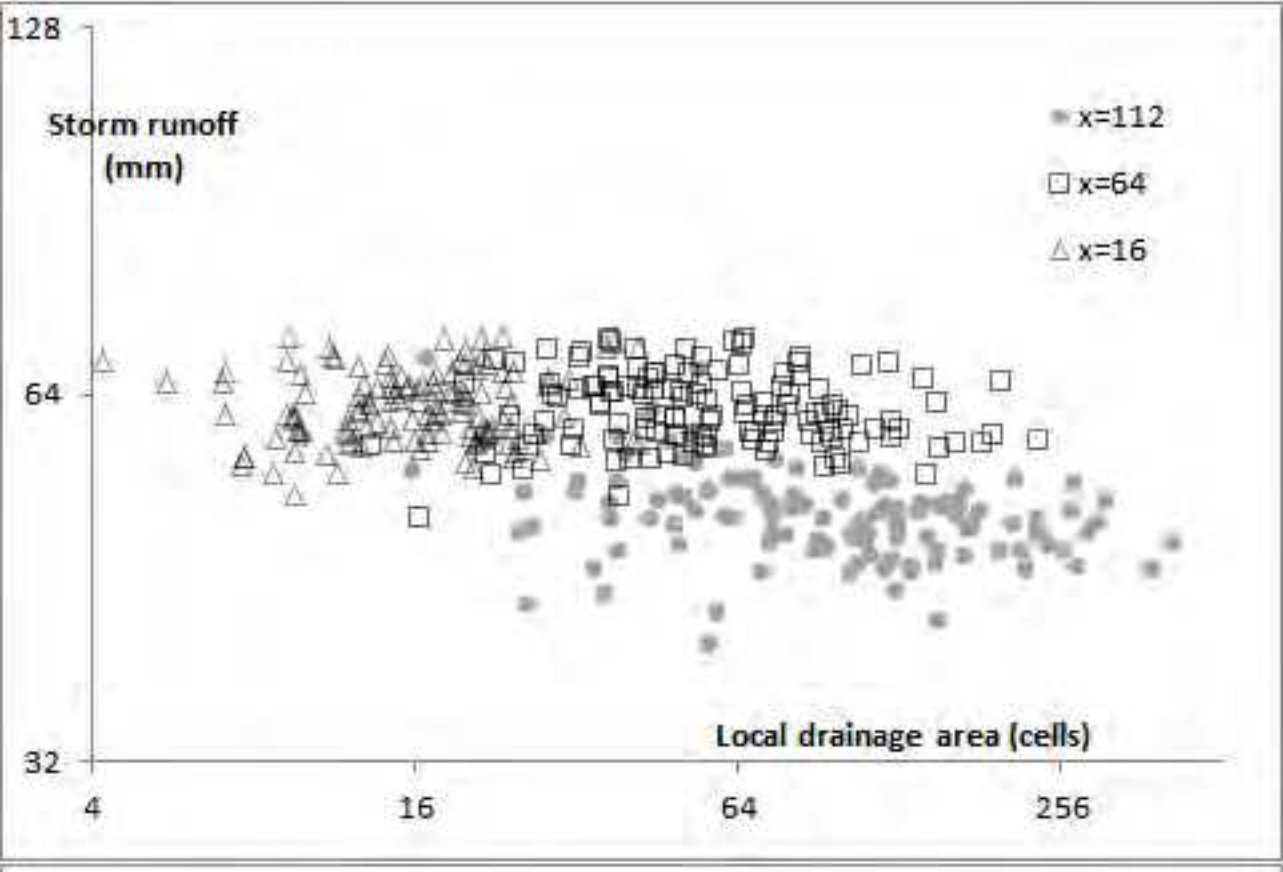
128
Storm runoff
(mm)
x=112
x=64
x=16
64
32
Local drainage area (cells)
4
16
64
256

(b)

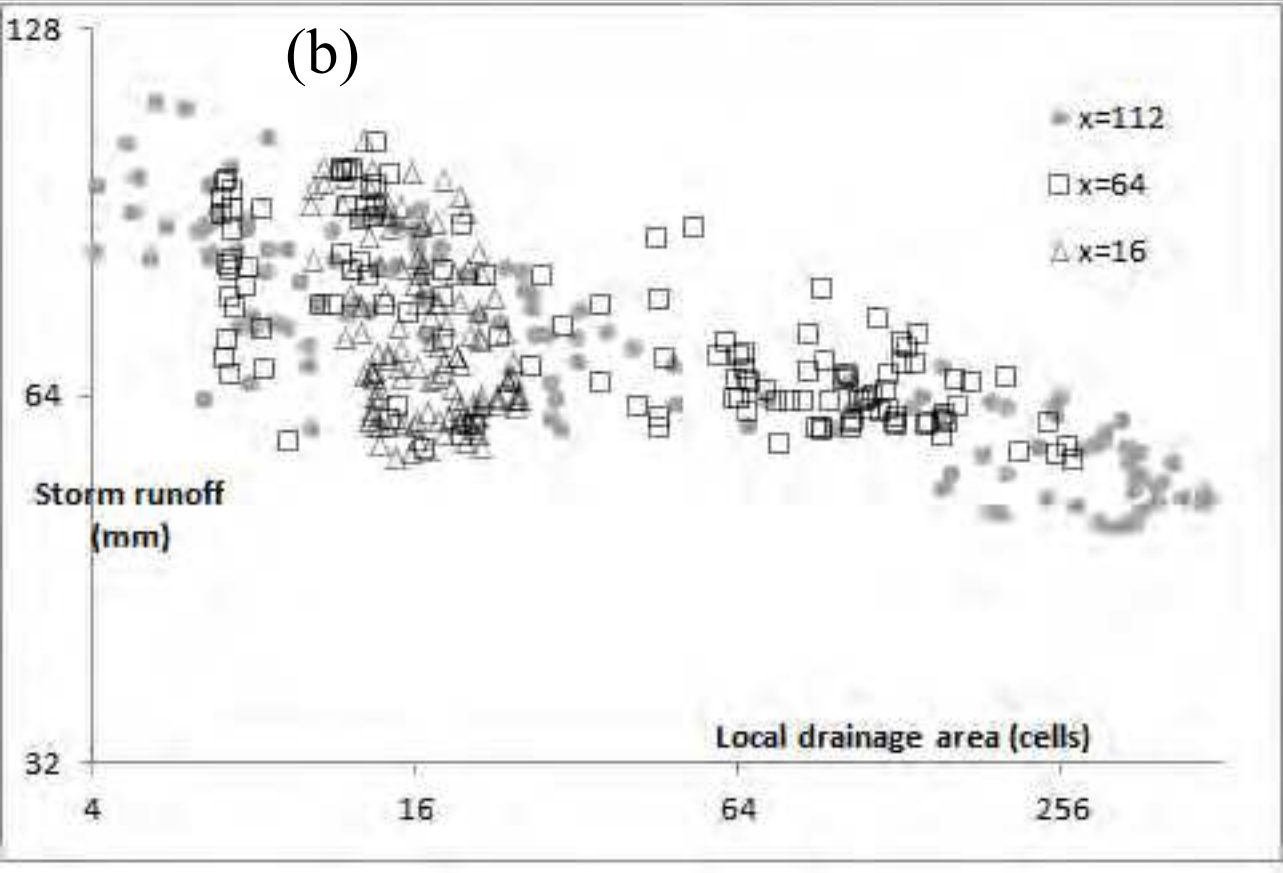
128
x=112
x=64
x=16
64
Storm runoff
(mm)
32
Local drainage area (cells)
4
16
64
256

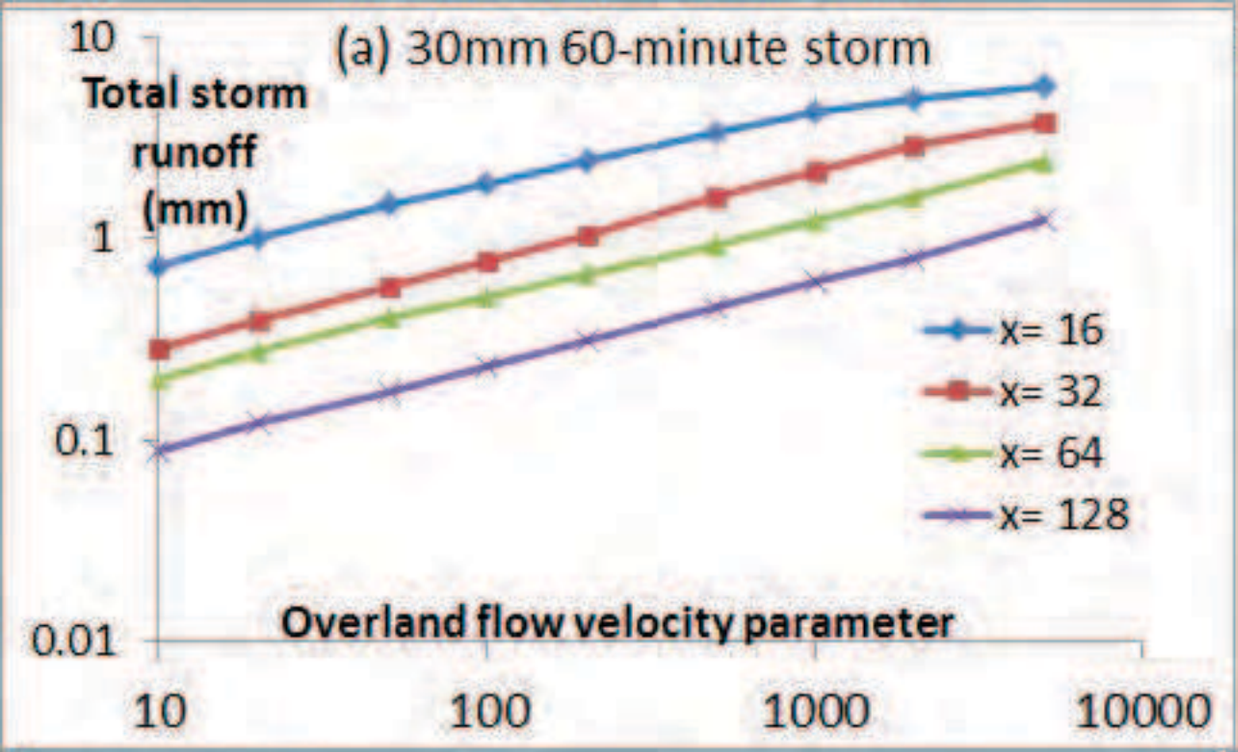
(a) 30mm 60-minute storm
Total storm runoff (mm)
10
1
0.1
0.01
Overland flow velocity parameter
10
100
1000
10000
x= 16
x= 32
x= 64
x= 128

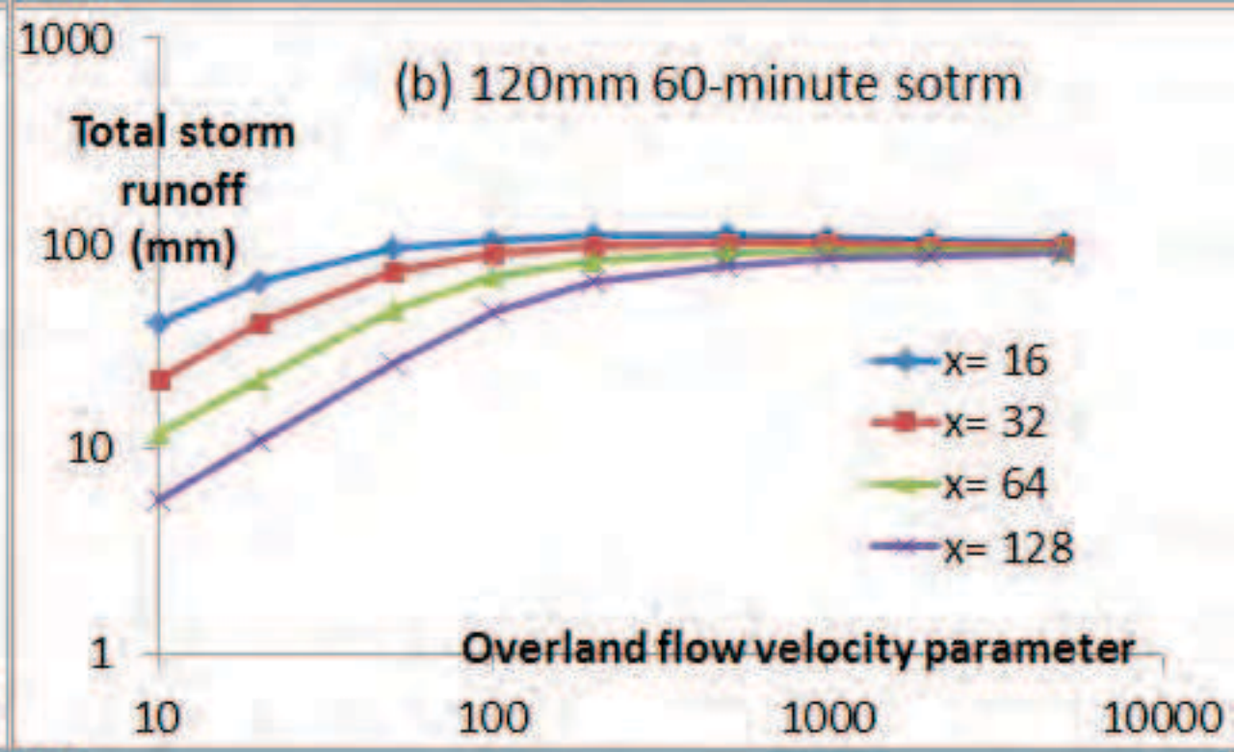
(b) 120mm 60-minute sotrm
Total storm runoff (mm)
1000
100
10
1
Overland flow velocity parameter
10
100
1000
10000
x= 16
x= 32
x= 64
x= 128

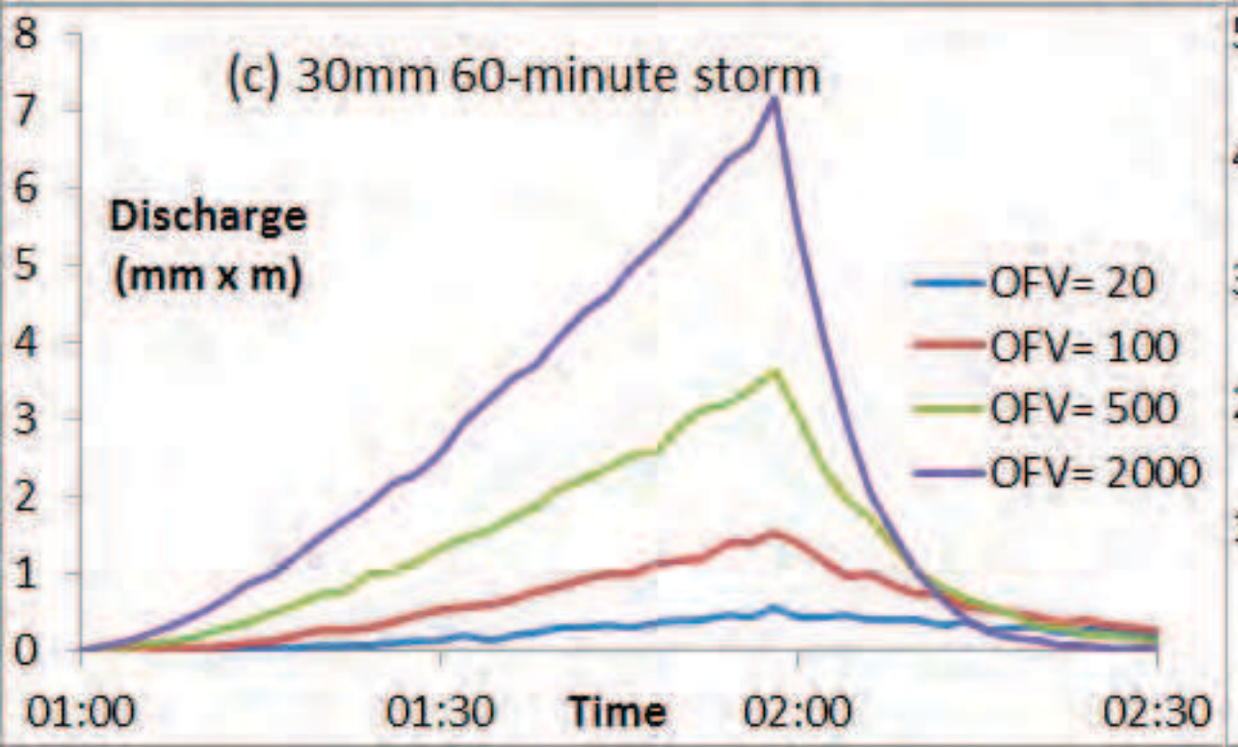
(c) 30mm 60-minute storm
Discharge (mm x m)
8
7
6
5
4
3
2
1
0
01:00
01:30
Time
02:00
02:30
OFV= 20
OFV= 100
OFV= 500
OFV= 2000

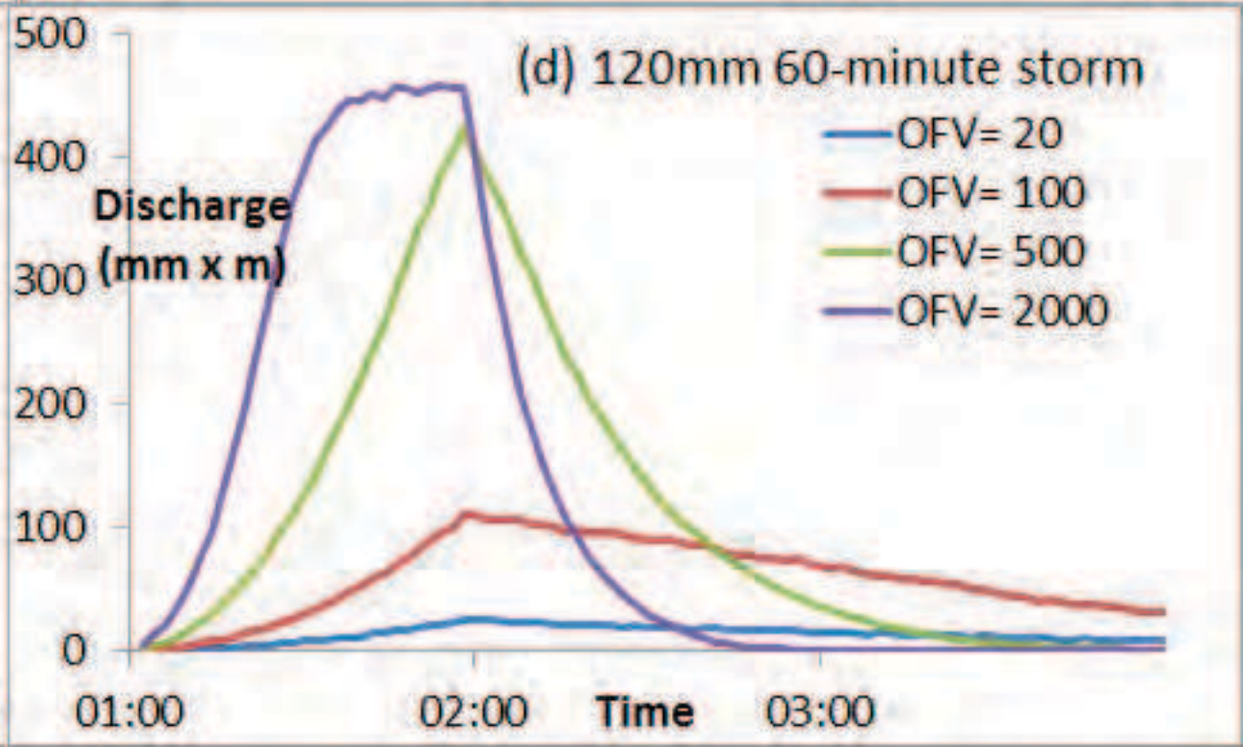
(d) 120mm 60-minute storm
Discharge (mm x m)
500
400
300
200
100
0
01:00
02:00
Time
03:00
OFV= 20
OFV= 100
OFV= 500
OFV= 2000

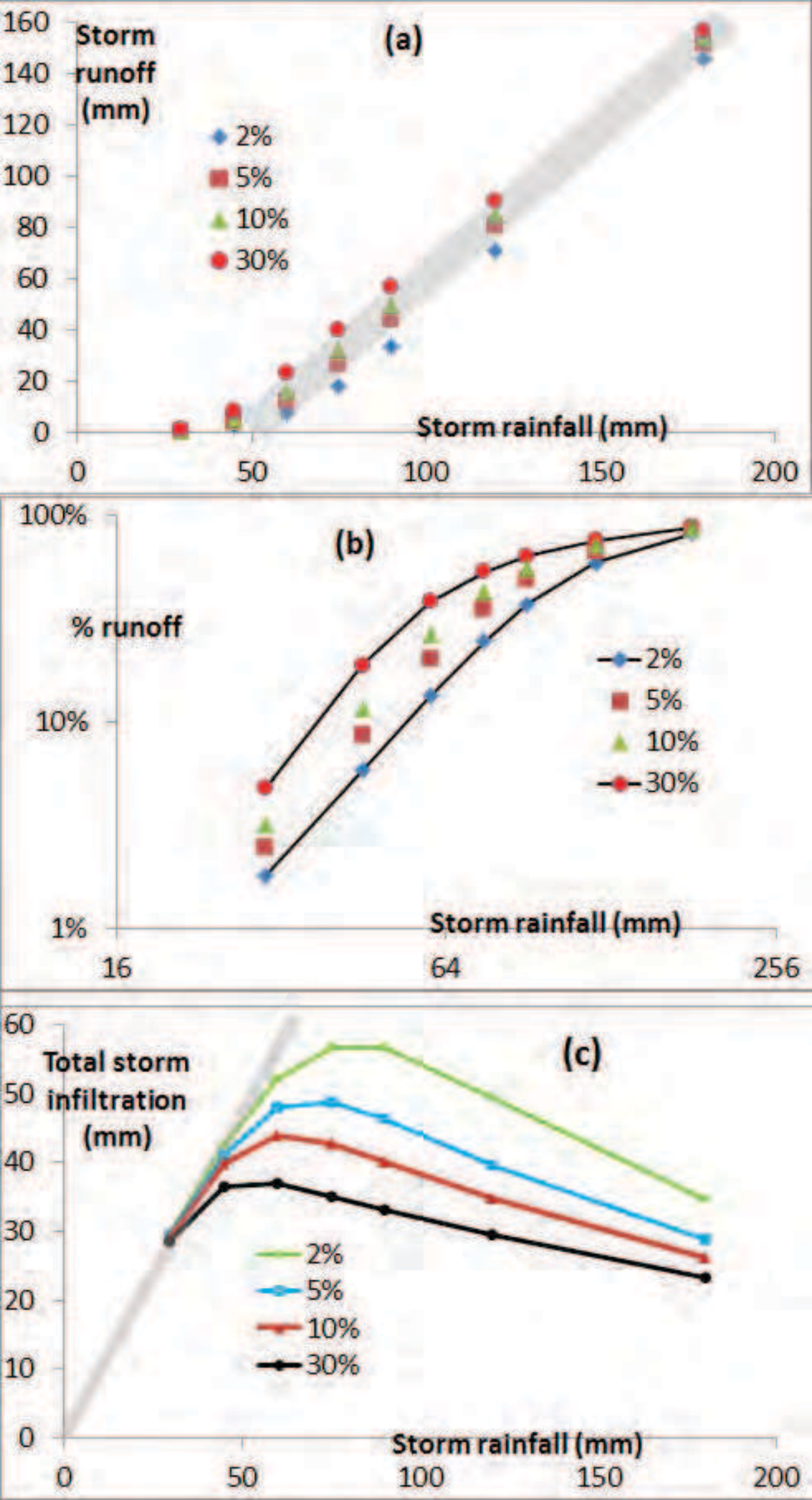
(a)
Storm runoff (mm)
160
140
120
100
80
60
40
20
0
2%
5%
10%
30%
Storm rainfall (mm)
0
50
100
150
200
(b)
100%
% runoff
10%
1%
2%
5%
10%
30%
Storm rainfall (mm)
16
64
256
(c)
Total storm infiltration (mm)
60
50
40
30
20
10
0
2%
5%
10%
30%
Storm rainfall (mm)
0
50
100
150
200

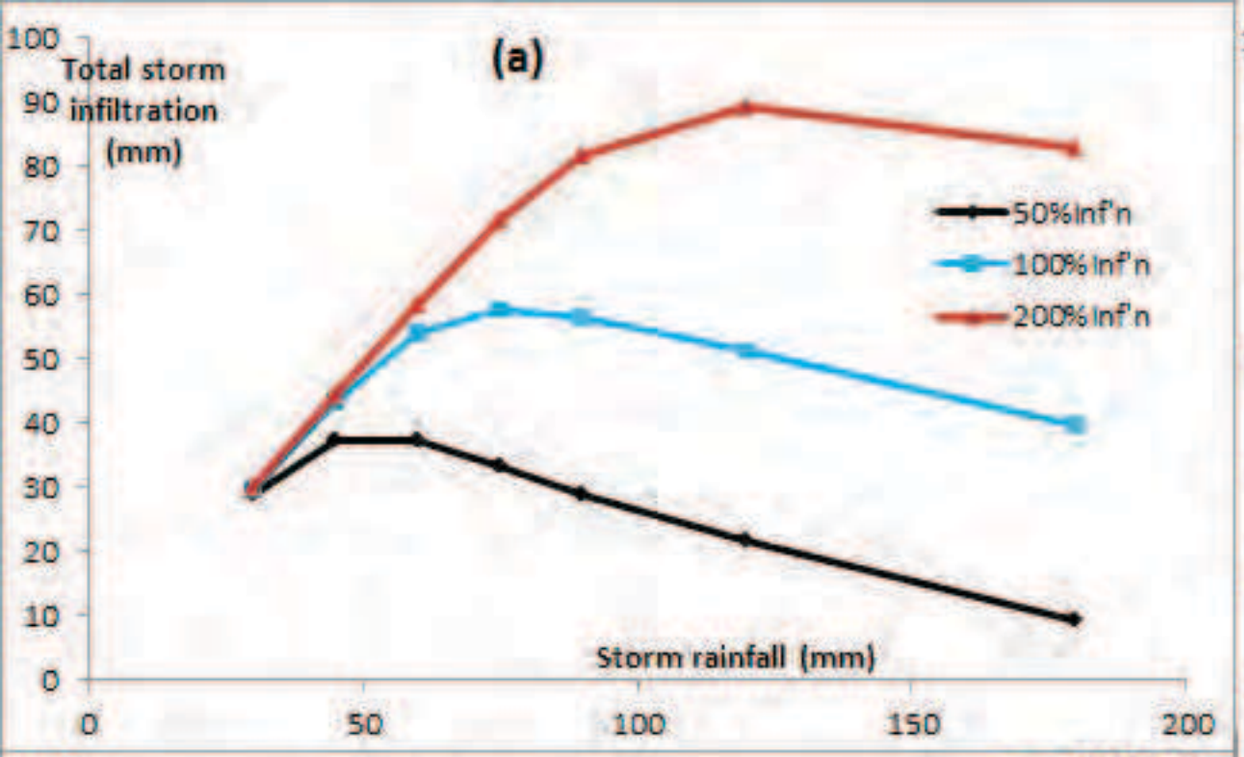
(a)
Total storm infiltration (mm)
Storm rainfall (mm)
50%Inf'n
100% Inf'n
200% Inf'n
0
10
20
30
40
50
60
70
80
90
100
0
50
100
150
200

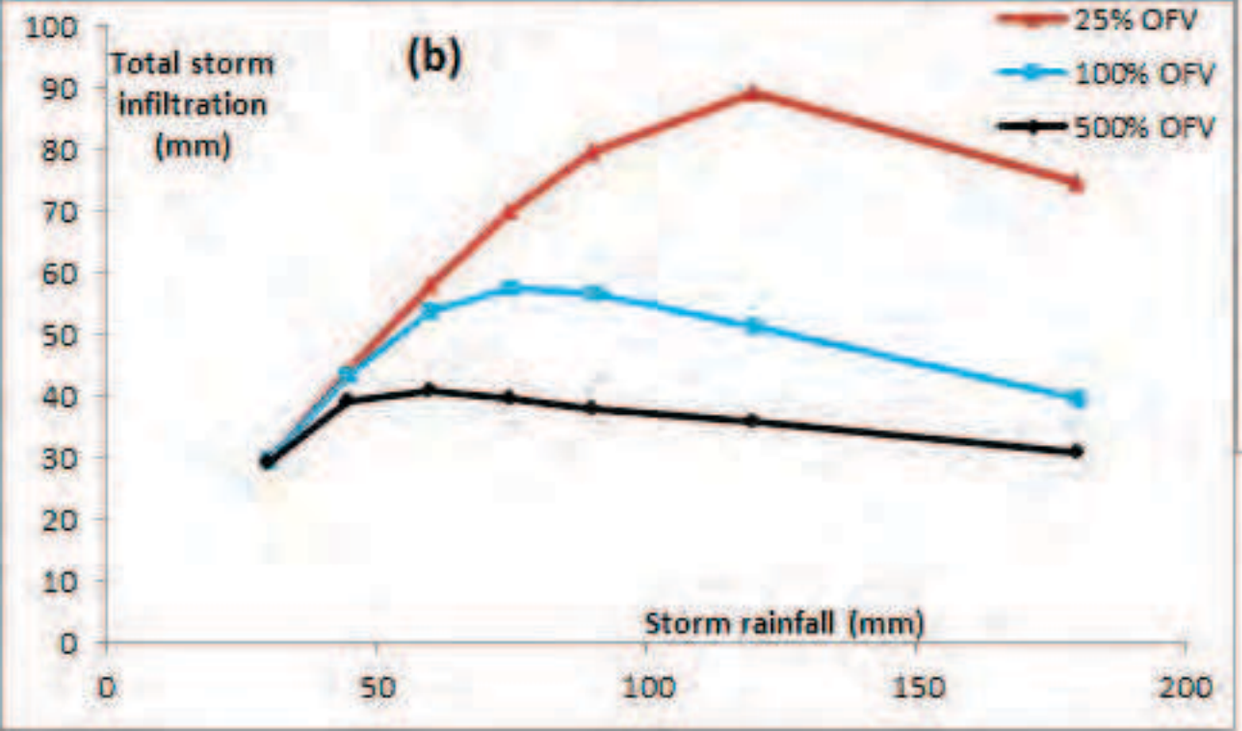
(b)
Total storm infiltration (mm)
Storm rainfall (mm)
25% OFV
100% OFV
500% OFV
0
10
20
30
40
50
60
70
80
90
100
0
50
100
150
200

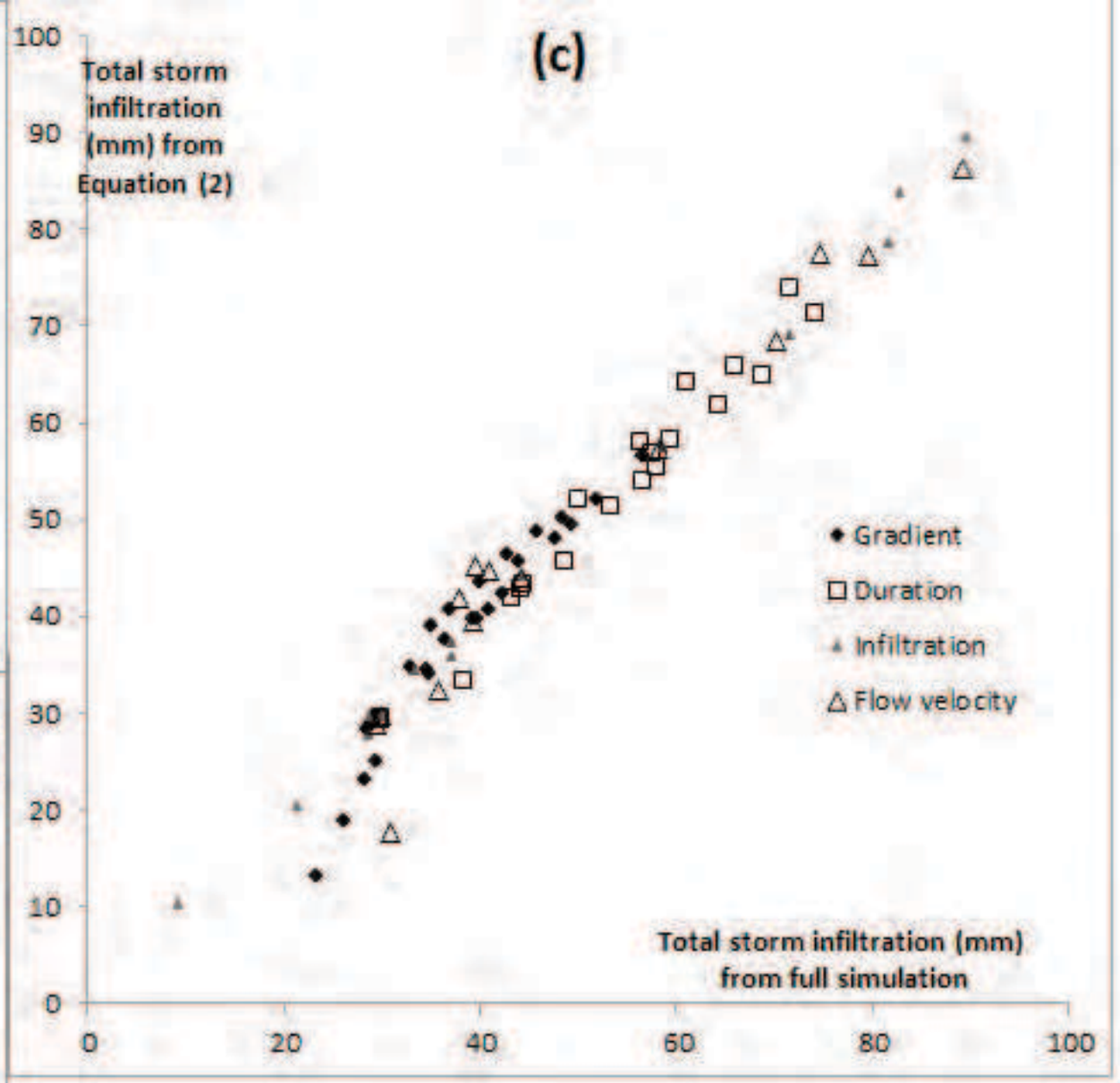
(c)
Total storm infiltration (mm) from Equation (2)
Total storm infiltration (mm) from full simulation
Gradient
Duration
Infiltration
Flow velocity
0
10
20
30
40
50
60
70
80
90
100
0
20
40
60
80
100

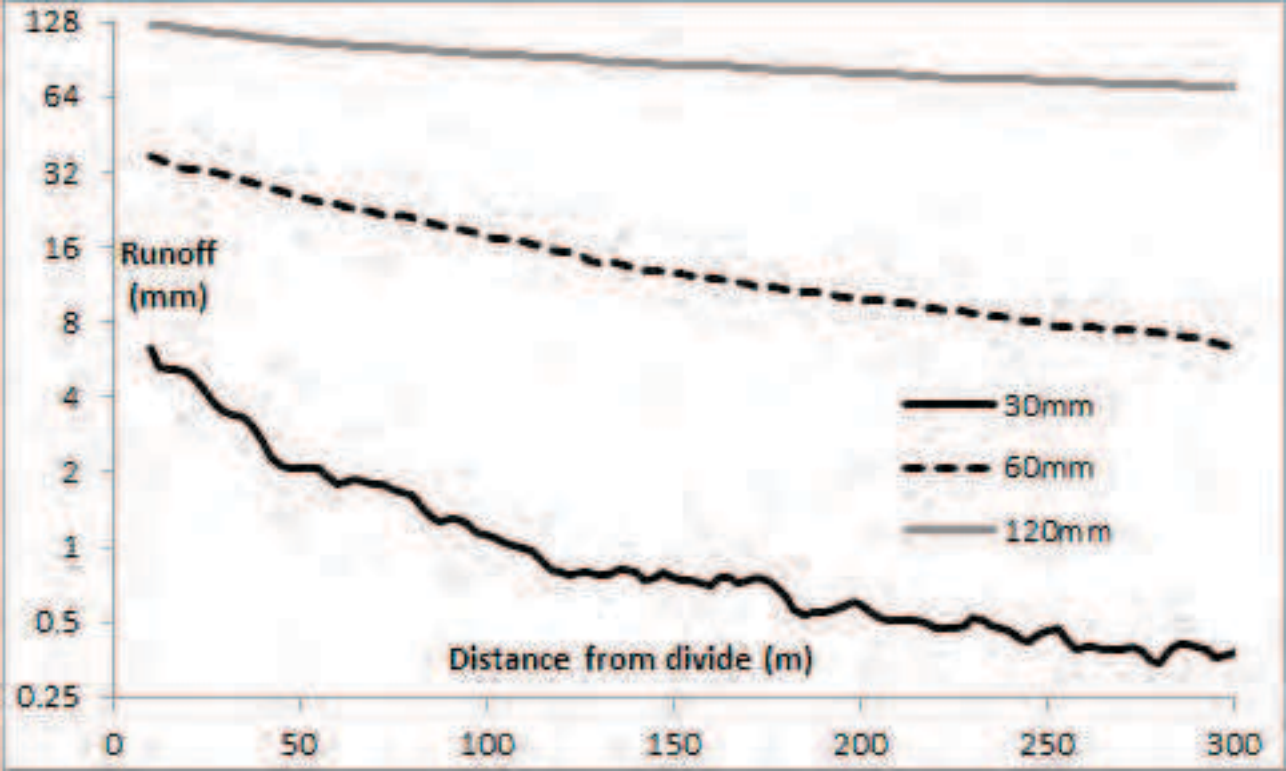
128
64
32
16
8
4
2
1
0.5
0.25
Runoff (mm)
30mm
60mm
120mm
Distance from divide (m)
0
50
100
150
200
250
300

(a) Uniform profile

Total storm infiltration (mm)

Storm rainfall (mm)

30minutes
60minutes
90minutes
120minutes

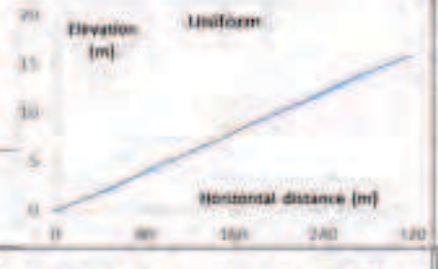

(b) Convex profile

Total storm infiltration (mm)

Storm rainfall (mm)

30minutes
60minutes
90minutes
120minutes

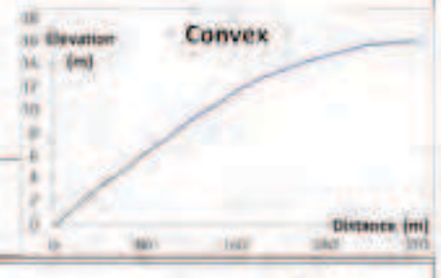

(c) Concave profile

Total Storm Infiltration (mm)

Storm rainfall (mm)

30minutes
60minutes
90minutes
120minutes

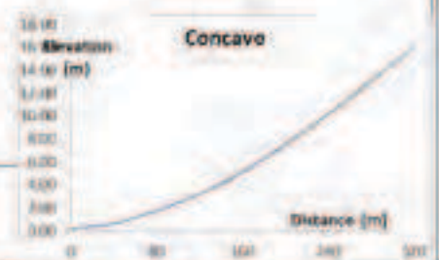

(d) Convexo-concave profile

Total storm infiltration (mm)

Storm rainfall (mm)

30minutes
60minutes
90minutes
120minutes

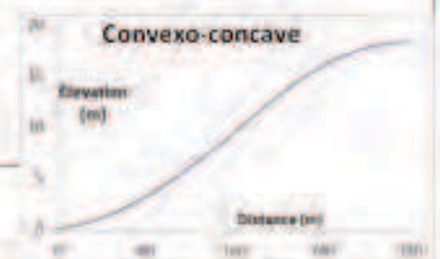

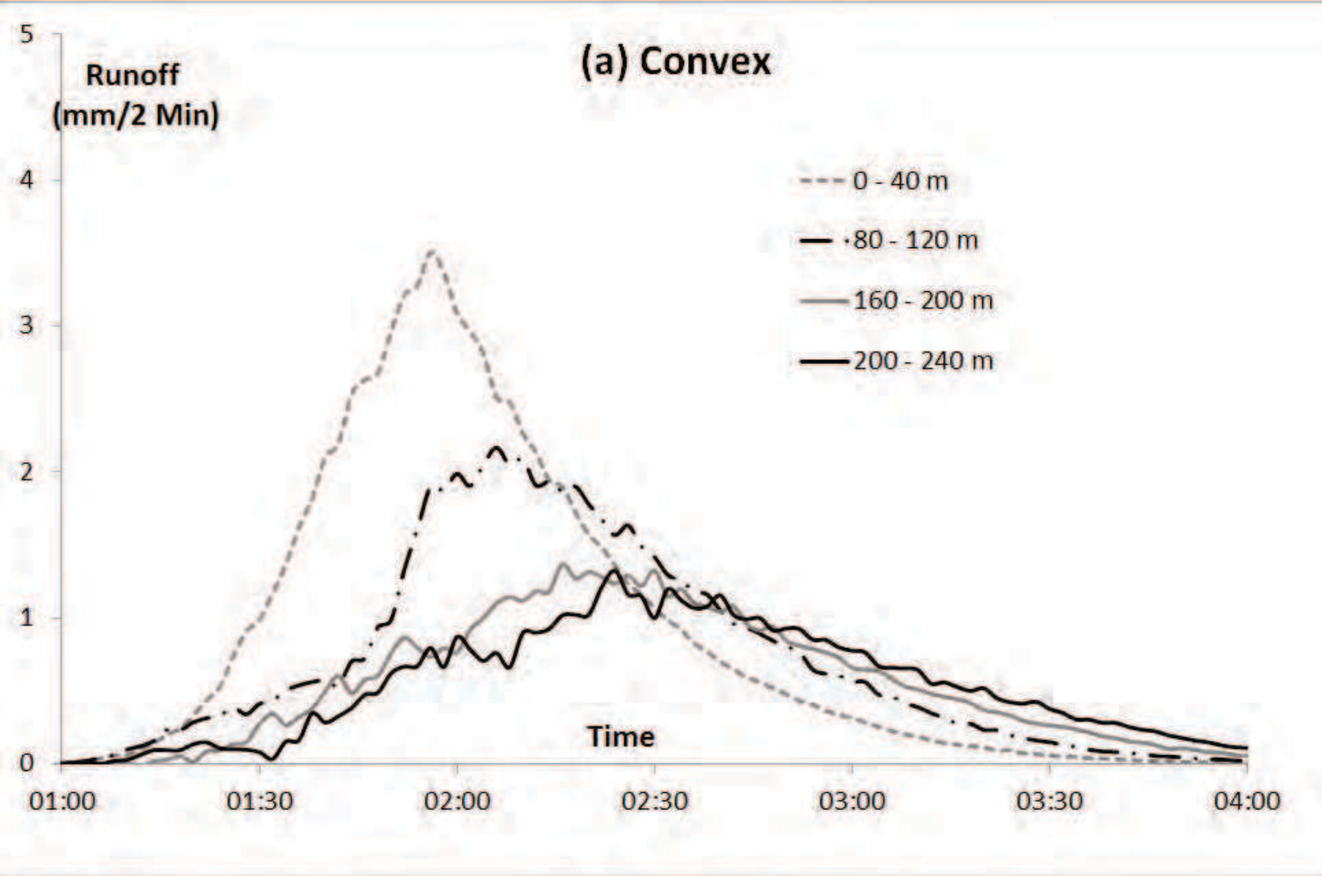
(a) Convex
Runoff
(mm/2 Min)
0 - 40 m
80 - 120 m
160 - 200 m
200 - 240 m
Time
0
1
2
3
4
5
01:00
01:30
02:00
02:30
03:00
03:30
04:00

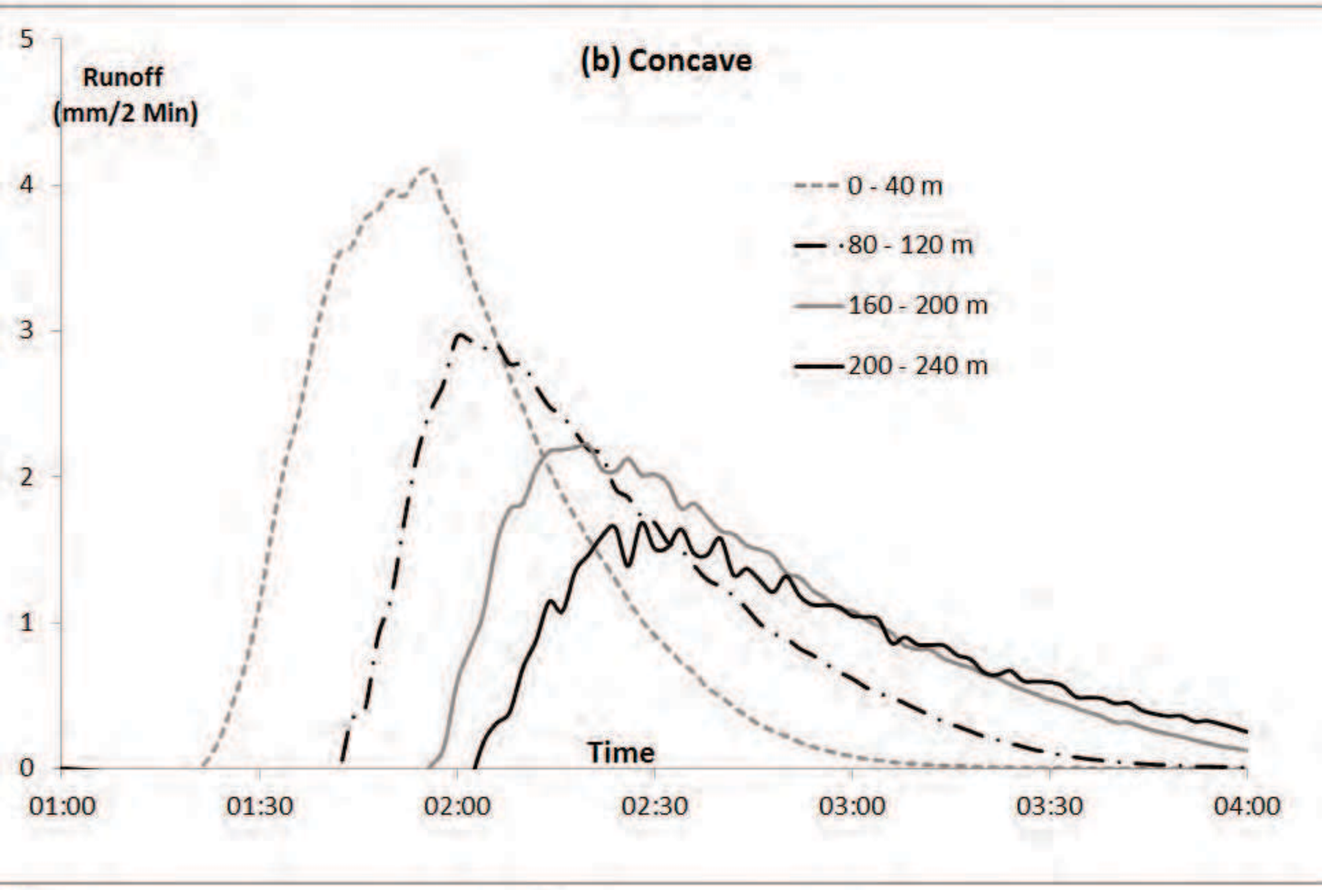
(b) Concave
Runoff
(mm/2 Min)
0 - 40 m
80 - 120 m
160 - 200 m
200 - 240 m
Time
0
1
2
3
4
5
01:00
01:30
02:00
02:30
03:00
03:30
04:00

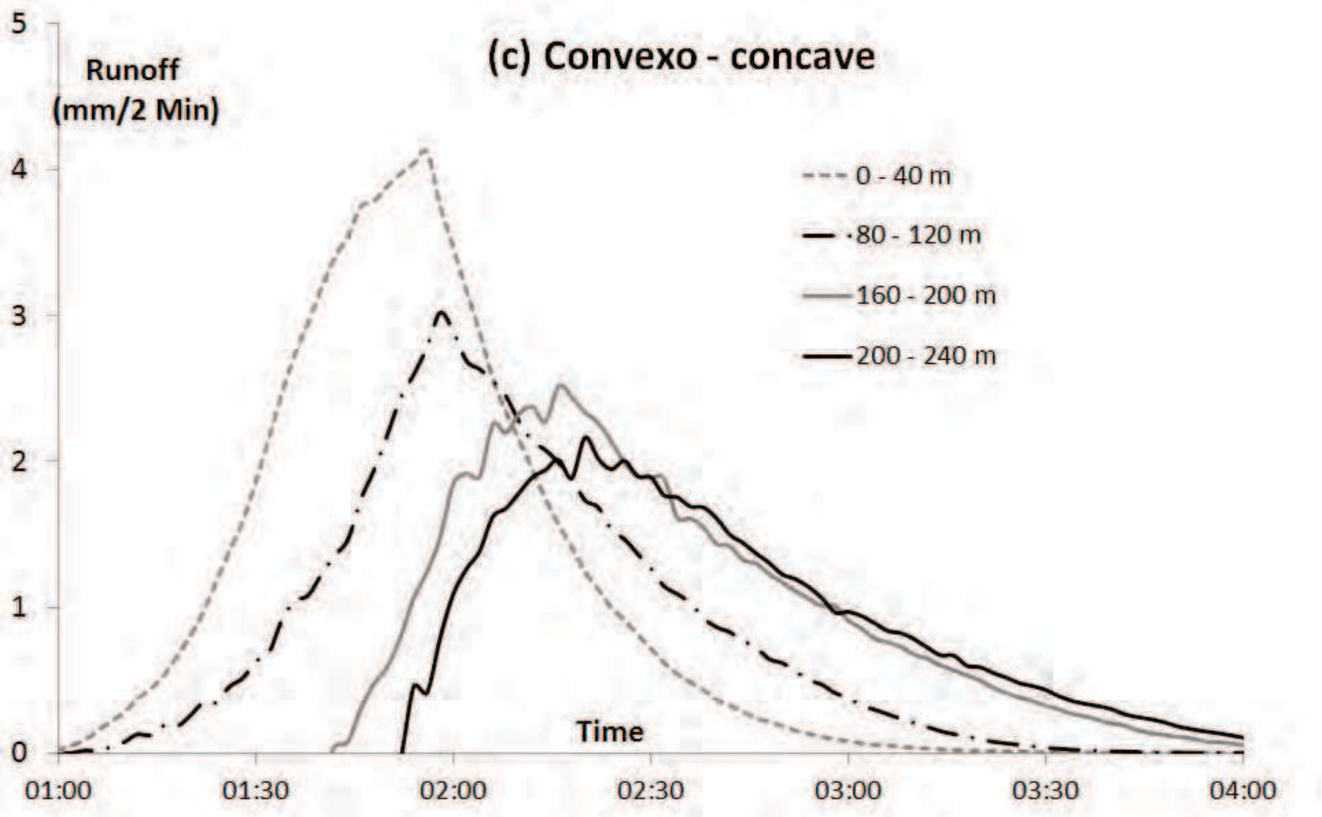
(c) Convexo - concave
Runoff
(mm/2 Min)
0 - 40 m
80 - 120 m
160 - 200 m
200 - 240 m
Time
0
1
2
3
4
5
01:00
01:30
02:00
02:30
03:00
03:30
04:00

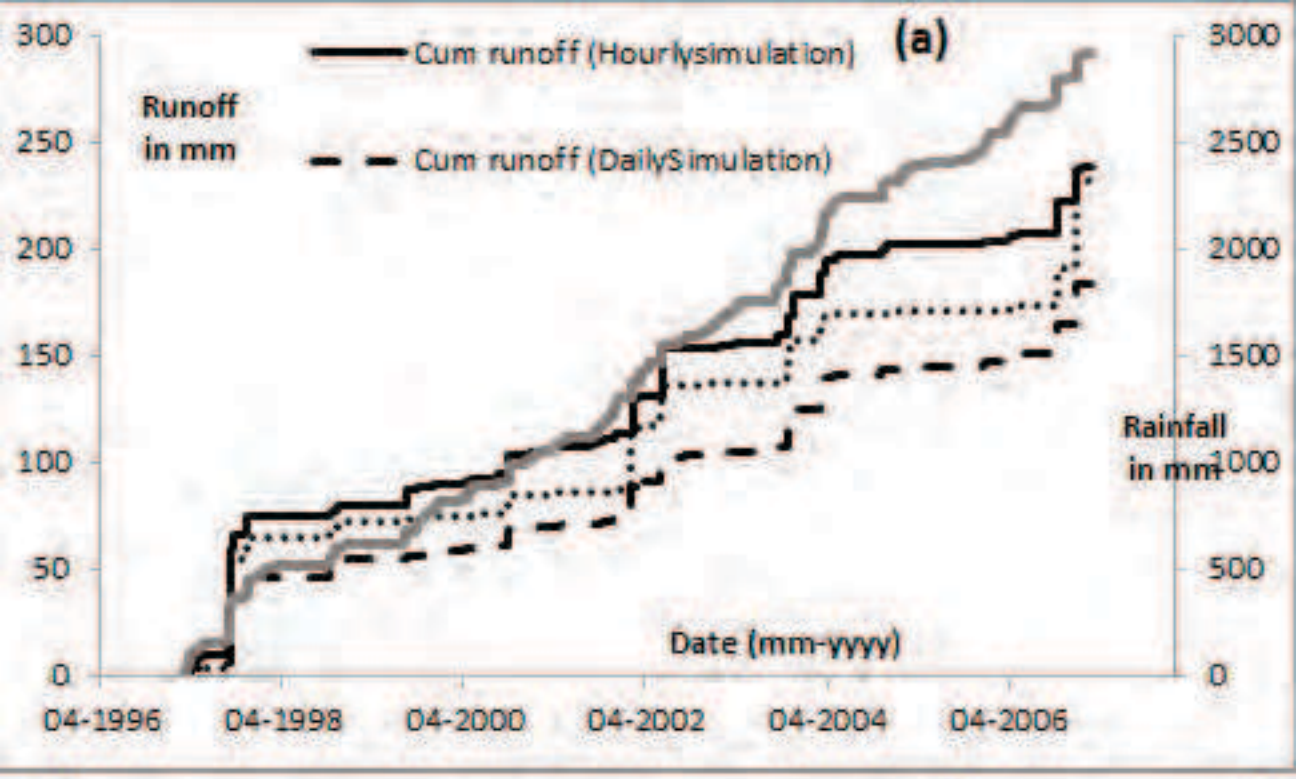
(a)
Cum runoff (Hourlysimulation)
Cum runoff (DailySimulation)
Runoff in mm
Rainfall in mm
Date (mm-yyyy)
300
250
200
150
100
50
0
3000
2500
2000
1500
1000
500
0
04-1996
04-1998
04-2000
04-2002
04-2004
04-2006

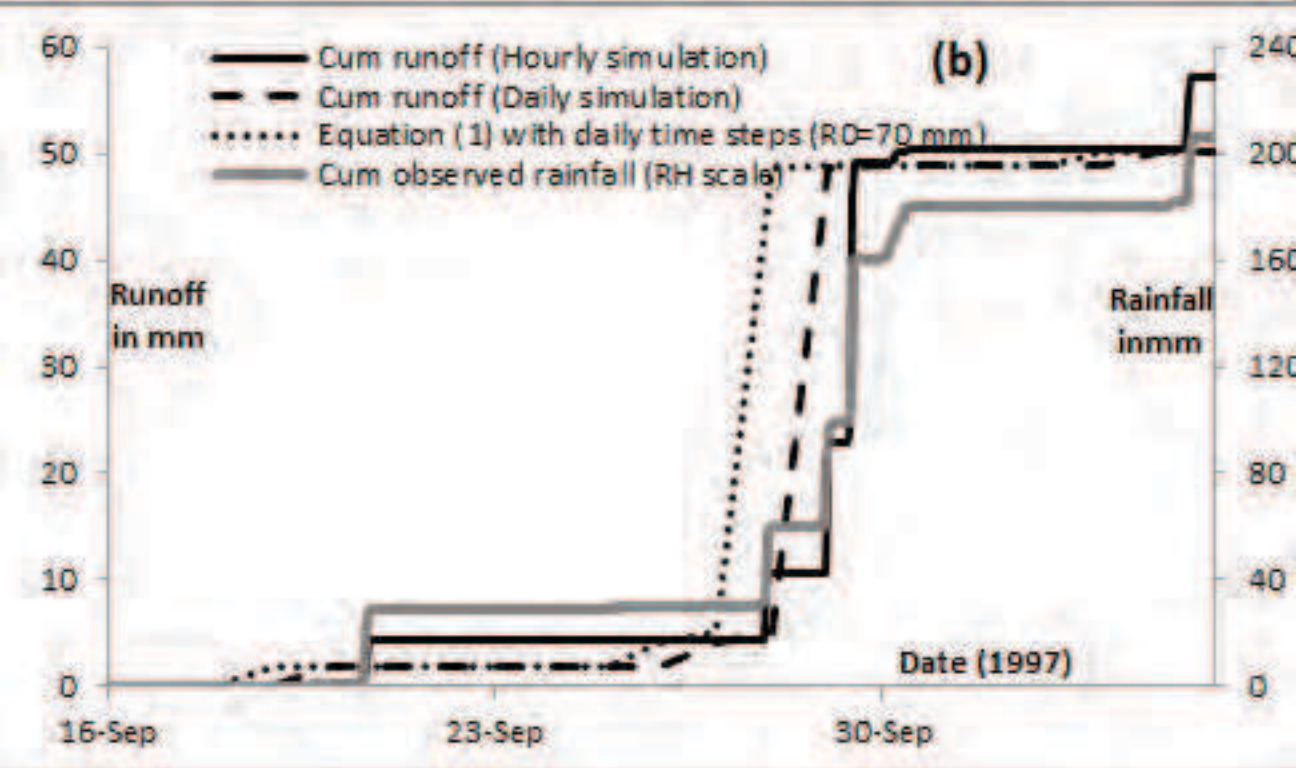
(b)
Cum runoff (Hourly simulation)
Cum runoff (Daily simulation)
Equation (1) with daily time steps (R0=70 mm)
Cum observed rainfall (RH scale)
Runoff in mm
Rainfall inmm
Date (1997)
60
50
40
30
20
10
0
240
200
160
120
80
40
0
16-Sep
23-Sep
30-Sep

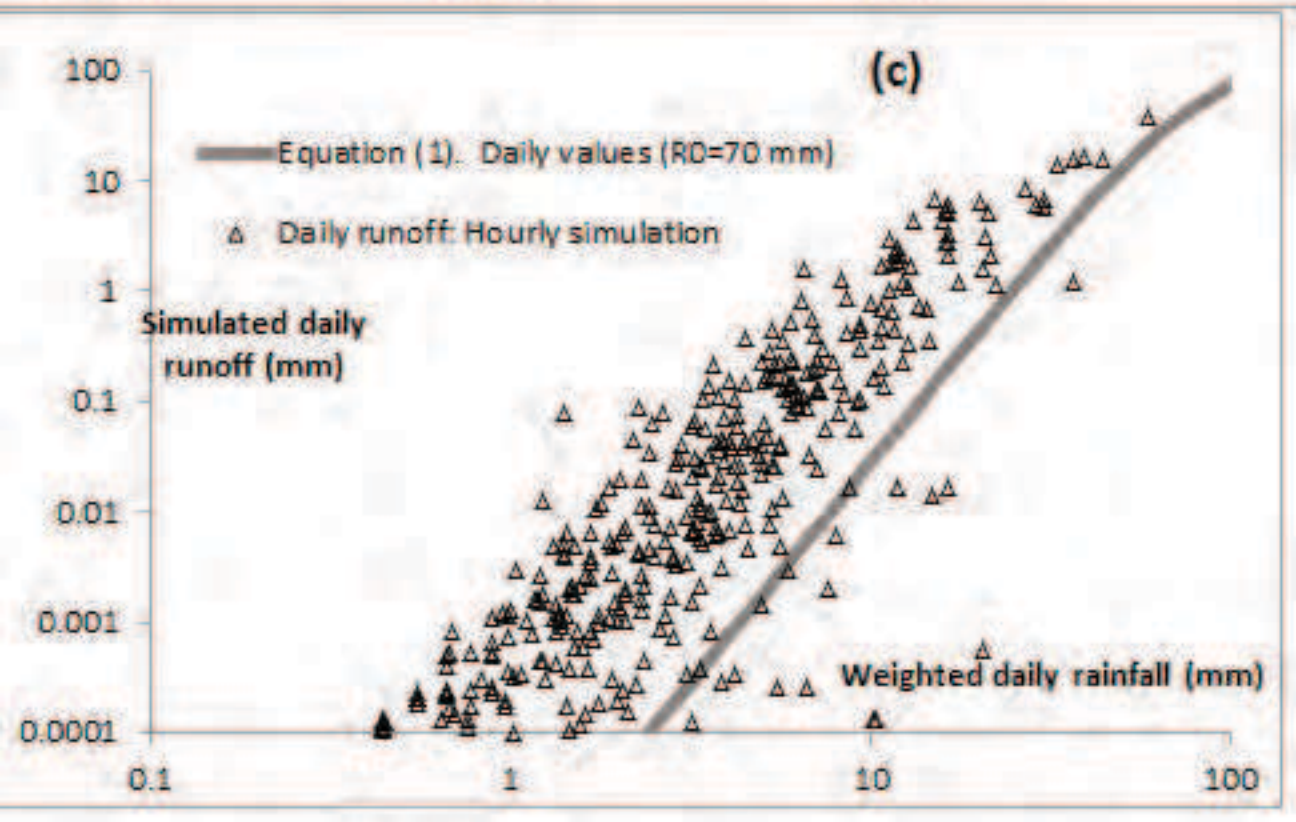
(c)
Equation (1). Daily values (R0=70 mm)
Daily runoff: Hourly simulation
Simulated daily runoff (mm)
Weighted daily rainfall (mm)
100
10
1
0.1
0.01
0.001
0.0001
0.1
1
10
100

(a)

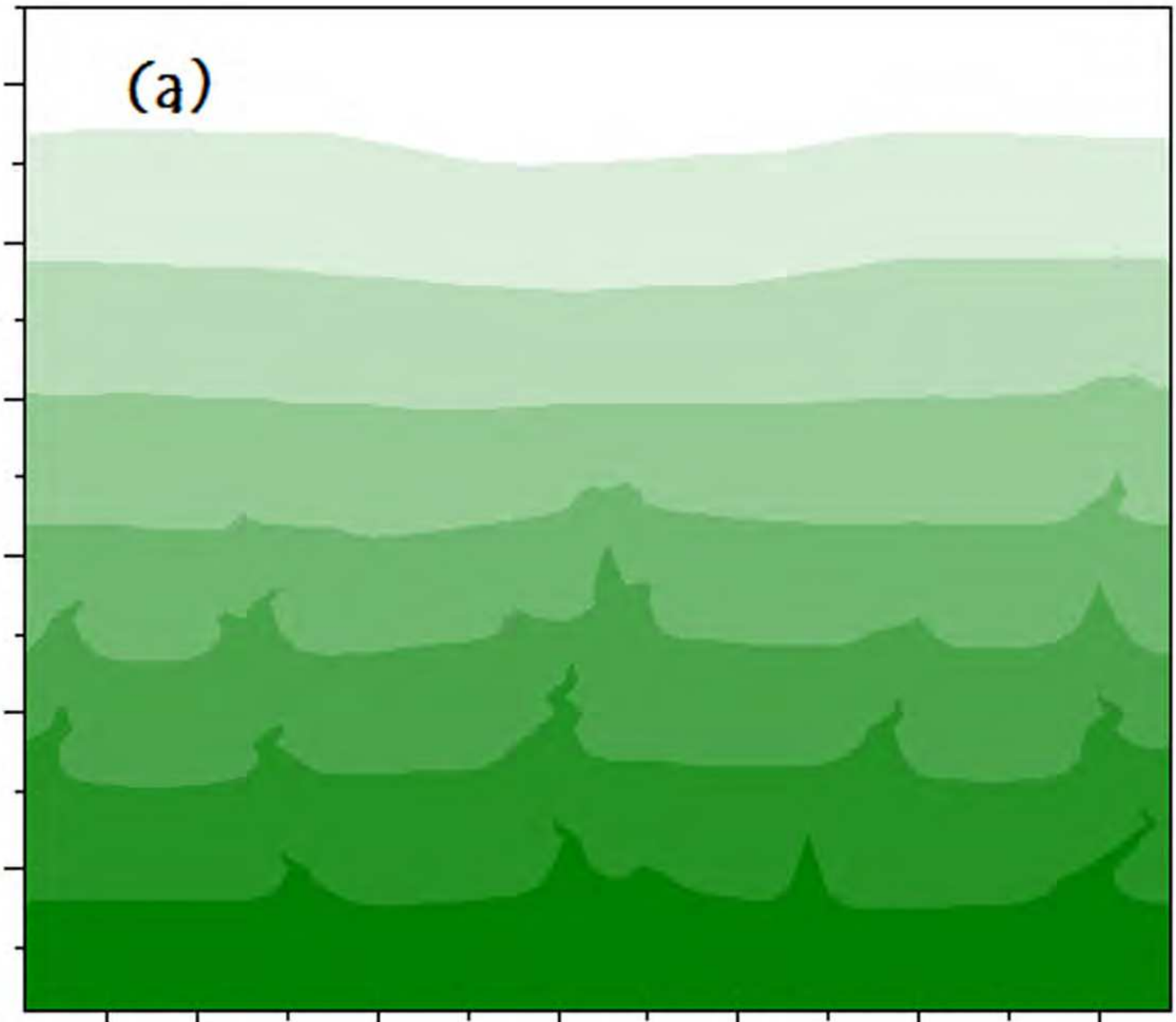

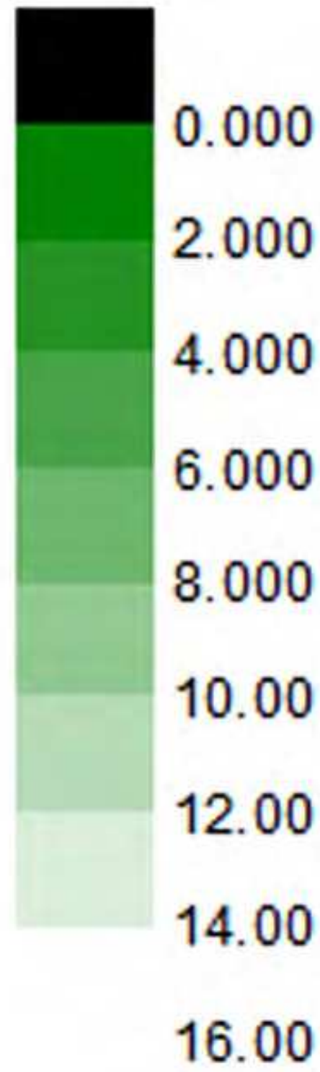
0.000
2.000
4.000
6.000
8.000
10.00
12.00
14.00
16.00

(b)

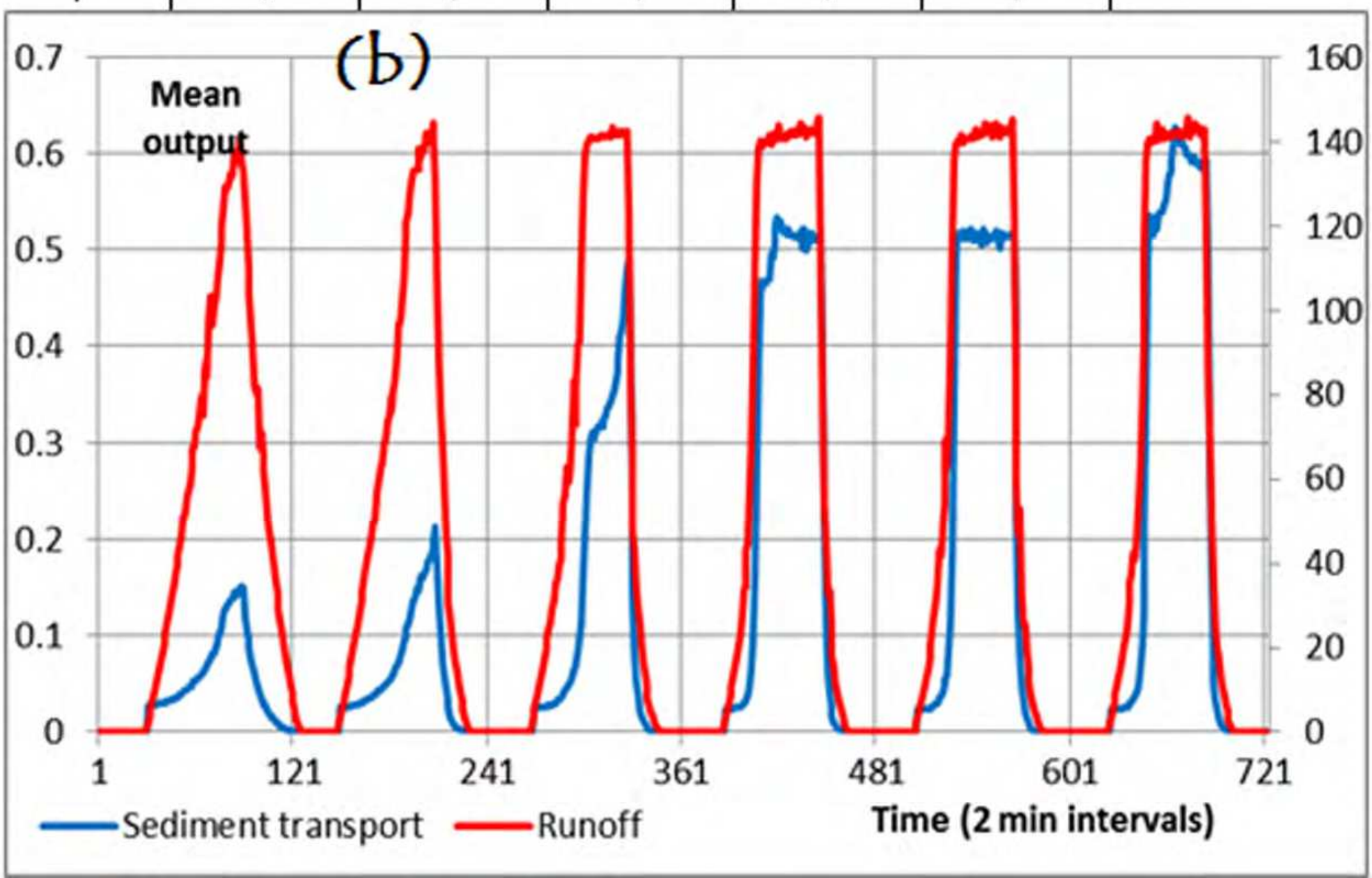
Mean output
0.7
0.6
0.5
0.4
0.3
0.2
0.1
0
160
140
120
100
80
60
40
20
0
1
121
241
361
481
601
721
Sediment transport
Runoff
Time (2 min intervals)